Nonlinear optimal control for the rotary double inverted pendulum

G. Rigatos[a,*] M. Abbaszadeh[b] P. Siano[c]

[a]Unit Industrial Autom.
Industrial Systems Inst.
26504, Patras, Greece
grigat@ieee.org

[b]Dept. ECS Eng.
Rensselaer Polytech. Inst.
12065, NY, USA
masouda@ualberta.ca

[c]Dept. of Innovation Systems
Univ. of Salerno
84084, Fisciano, Italy
psiano@unisa.it

G. Cuccurullo[d] J. Pomares[e] B. Sari[f]

Dept. of Industrial Eng.
Univ. of Salerno
84084, Fisciaano, Italy
gcuccurullo@unisa.it

[e]Dept. of Systems Eng.
Univ. of Alicante
03690, Alicante, Spain
jpomares@gcloud.ua.es

[f]Dept of Electrical Eng.
University of Setif
Setif, 19000, Algeria
bilal.sari@univ-setif.dz

Abstract: The control problem of the rotary double inverted pendulum (double Furuta pendulum) is nontrivial because of underactuation and strong nonlinearities in the associated state-space model. The system has three degrees of freedom (one actuated and two unactuated joints) while receiving only one control input. In this article, a novel nonlinear optimal (H-infinity) control approach is developed for the dynamic model of the rotary double inverted pendulum. First, the dynamic model of the double pendulum undergoes approximate linearization with the use of first-order Taylor series expansion and through the computation of the associated Jacobian matrices. The linearization process takes place at each sampling instance around a temporary operating point which is defined by the present value of the system's state vector and by the last sampled value of the control inputs vector. At a next stage a stabilizing H-infinity feedback controller is designed. To compute the controller's feedback gains an algebraic Riccati equation has to be solved at each time-step of the control algorithm. The global stability properties of the control scheme are proven through Lyapunov analysis. To implement state estimation-based control without the need to measure the entire state vector of the rotary double-pendulum the H-infinity Kalman Filter is used as a robust state observer. The nonlinear optimal control method achieves fast and accurate tracking of setpoints by all state variables of the rotary double inverted pendulum under moderate variations of the control input.

Keywords: rotary double inverted pendulum, underactuated systems, approximate linearization, Taylor series expansion, Jacobian matrices, H-infinity control, Riccati equation, global stability, Lyapunov analysis.

1 Introduction

Nonlinear control for underactuated robotic systems is an elaborated task which has become the subject of much research work during the last years [1-4]. In this domain, the double rotary pendulum (double

*Corresponding author

This article has been accepted for publication and undergone full peer review but has not been through the copyediting, typesetting, pagination and proofreading process which may lead to differences between this version and the Version of Record. Please cite this article as doi: 10.1002/adc2.140

Furuta pendulum) is a benchmark nonlinear dynamical system and the solution of the associated nonlinear optimal control problem is challenging [5-9]. Actually, stabilization of the dynamics of the double rotary pendulum is a nontrivial task because of the strong nonlinearities of the associated state-space model and because of the model's underactuation [46-12]. Out of the three joints of the pendulum only one receives mechanical actuation, and this makes significantly difficult the control of the pendulum and its stabilization at the swing-up position [13-15]. So far, several control approaches have been proposed for the model of the double rotary pendulum. These include control based on LQR concepts and approaches based on Linear Parameter Varying formulations of the system's dynamics, as well as on the solution of state-dependent Riccati equations [16-20]. One also finds sliding-mode and backstepping control approaches. Additionally, there are optimal control concepts which often take the form of Model Predictive Control schemes [21-25]. It is noted that the solution of the nonlinear control problem for the rotary double inverted pendulum provides also an insight for the successful implementation of stabilizing feedback in several highly nonlinear and underactuated robotic systems [26- 28].

In this article, a novel nonlinear optimal (H-infinity) control method is proposed for the complex dynamics of the rotary double inverted pendulum [40]. First, the dynamic model of the rotary double inverted pendulum undergoes approximate linearization around a temporary operating point which is updated at each sampling instance. This operating point is defined at each sampling period by the present value of the pendulum's state vector and by the last sampled value of the control inputs vector. The linearization process is based on first-order Taylor series expansion and on the computation of the associated Jacobian matrices [41-43]. The model imprecision which is due to the truncation of higher-order terms from the Taylor series expansion is treated as a perturbation which is asymptotically compensated by the robustness of the control algorithm. For the approximately linearized model of the rotary double inverted pendulum a stabilizing H-infinity feedback controller is designed. This controller achieves the solution of the optimal control problem for the nonlinear dynamics of the rotary double inverted pendulum under model uncertainty and external disturbances [2-4].

Actually, the H-infinity controller represents a min-max differential game which takes place between: (i) the system's control inputs that try to minimize a cost function which contains a quadratic term of the state vector's tracking error, (ii) the system's disturbances and model uncertainty terms which try to maximize this cost function. To select the feedback gains of the H-infinity controller an algebraic Riccati equation has to be repetitively solved at each time-step of the control algorithm [1-4]. The global stability properties of the control scheme are proven through Lyapunov analysis. First, it is demonstrated that the control loop of the rotary double inverted pendulum satisfies the H-infinity tracking performance criterion [1-4],[44]. This signifies elevated robustness against model uncertainty and exogenous perturbations. Moreover, under moderate conditions global asymptotic stability properties are proven [1-4]. To implement also state estimation-based control without the need to measure the entire state-vector of the rotary double inverted pendulum, the H-infinity Kalman Filter is proposed as a robust state observer. The article's nonlinear optimal (H-infinity) control scheme achieves fast and accurate tracking of reference setpoints under moderate variations of the control inputs. The control problem of rotary single and double inverted pendulum can be used as a benchmark for testing linear and nonlinear control algorithms, and the results of the present article confirm that the proposed nonlinear optimal control method is a meaningful contribution to the research area of nonlinear control [29- 34]. The use of the article's nonlinear optimal control method can be extended to more nonlinear underactuated dynamical systems which have been the subject of control systems research during the last years [35-39].

A comparison of the nonlinear optimal (H-infinity) control method against other linear and nonlinear control schemes for complex dynamical systems has shown the following: (1) unlike Lie algebra-based control, the new nonlinear optimal control method does not rely on complicated transformations (diffeomorphisms) of the system's state variables. The control inputs that the nonlinear optimal control method computes can be applied directly to the initial nonlinear dynamics of the system and are not used on its transformed

equivalent description. The inverse transformations which are met in global linearization-based control are avoided and consequently one does not come against singularity issues (2) unlike Model Predictive Control and Nonlinear Model Predictive Control the nonlinear optimal control method is of proven global stability. It is known that Model Predictive Control is a linear control method which if applied to systems with complex nonlinear dynamics the stability of the control loop will be lost. Besides, in Nonlinear Model Predictive Control the convergence of the iterative search for an optimum depends on initialization and parameter values selection and consequently the global stability properties of the NMPC method cannot be ensured either (2) unlike sliding-mode and backstepping control the nonlinear optimal control method does not require the state-space description of the system to be found in a specific form. About sliding-mode control it is known that when the controlled system is not found in the input-output linearized form, the definition of the sliding surface can be an intuitive procedure. About backstepping control it is known that it cannot be directly applied to a dynamical system if the related state-space model is not found in the strict-feedback (backstepping integral) form (4) unlike PID control, the nonlinear optimal control method is of proven global stability, the selection of the controller's parameters does not rely on a heuristics-based tuning procedure and the stability of the control loop is ensured in case of changes of operating points (5) unlike multiple local models-based control, the nonlinear optimal control method uses only one linearization point and needs the solution of only one Riccati equation so as to compute the stabilizing feedback gains of the controller. Equivalently, the nonlinear optimal control method does not require the solution of complicated Linear Matrix Inequalities. Consequently, in terms of computation load the nonlinear optimal control method is much more efficient.

The structure of the article is as follows: in Section 2 the dynamic model of the rotary double inverted pendulum is formulated and the associated state-space description is obtained. In Section 3 the dynamic model of the rotary double inverted pendulum is subjected to approximate linearization through first-order Taylor series expansion and through the computation of the associated Jacobian matrices. In Section 4 an H-infinity controller is designed to stabilize the dynamics of the rotary double inverted pendulum. In Section 5 the global stability properties of the nonlinear optimal (h-infinity) control scheme are proven through Lyapunov analysis. In Section 6 the use of the nonlinear optimal control method is also extended to the dynamic model of the parallel double inverted pendulum. In Section 7 the performance of the control loop for the rotary double inverted pendulum is confirmed through simulation experiments. Besides the fine performance of the nonlinear optimal control method is also confirmed in the case of the parallel double inverted pendulum. Finally, in Section 8 concluding remarks are stated.

2 Dynamic model of the double rotary pendulum

The diagram of the rotary double inverted pendulum is shown in Fig. 1. The state vector of the system consists of the turn angles of the rigid links and of the associated angular velocities, that is $x = [\theta_0, \dot{\theta}_0, \theta_1, \dot{\theta}_1, \theta_2, \dot{\theta}_2]^T$. The rotary double inverted pendulum is underactuated since mechanical torque is applied only to the first link. Thus the torques vector is $\tau = [T_1, 0, 0]^T$. Main parameters of the dynamic model of the rotary double inverted pendulum are: $l_i,\ i = 0, 1, 2$ which are the lengths of the links, $r_i,\ i = 0, 1, 2$ which are the distances between the joint at the basis of the links and the center of gravity of the links and $m_i,\ i = 0, 1, 2$ are the masses of the links. [5-9]. The dynamic model of the system is given by

$$M(\theta)\ddot{\theta} + H(\theta, \dot{\theta})\dot{\theta} + G(\theta) = \tau \tag{1}$$

The inertia matrix of the rotary double inverted pendulum is symmetric and positive definite and is given by [5]

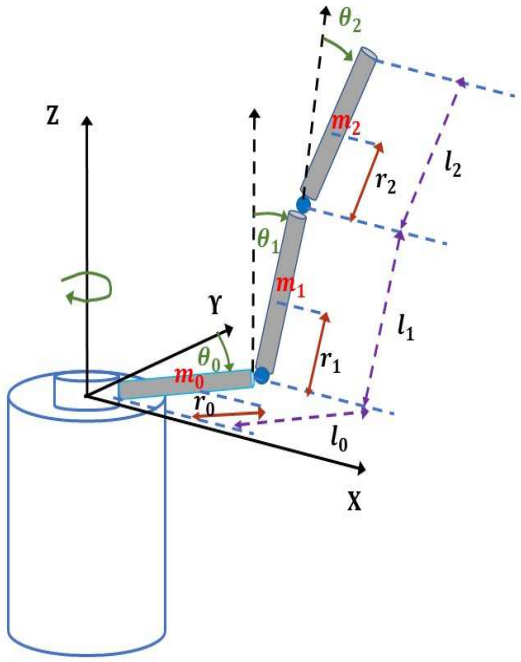

Figure 1: Diagram of the rotary double inverted pendulum

$$M(\theta) = \begin{pmatrix} m_{11} & m_{12} & m_{13} \\ m_{21} & m_{22} & m_{33} \\ m_{31} & m_{32} & m_{33} \end{pmatrix} \tag{2}$$

where $m_{11} = J_0 + (m_1 + m_2)l_0^2 + (m_1 r_1^2 + m_2 l_1^2)sin^2(\theta_1) + 2m_2 l_1 r_2 sin(\theta_1)sin(\theta_1 + \theta_2) + m_2 r_2^2 sin^2(\theta_1 + \theta_2)$, $m_{12} = m_{21} = m_1 l_0 r_1 cos(\theta_1) + m_2 l_0 r_2 cos(\theta_1 + \theta_2) + m_2 l_0 l_1 cos(\theta_1)$, $m_{13} = m_{31} = m_2 l_0 r_2 cos(\theta_1 + \theta_2)$, $m_{22} = J_1 + J_2 + m_1 r_1^2 + m_2 l_1^2 + m_2 r_2^2 + 2m_2 l_1 r_2^2 + 2m_2 l_1 r_2 cos(\theta_2)$, $m_{23} = m_{32} = J_2 + m_2 r_2^2 + m_2 l_1 r_2 cos(\theta_2)$, $m_{33} = J_2 + m_2 r_2^2$.

The Coriolis forces vector of the system is given by $C(\theta, \dot{\theta}) = H(\theta, \dot{\theta})\dot{\theta}$ where matrix $H(\theta, \dot{\theta})$ is given by [5]

$$H(\theta.\dot{\theta}) = \begin{pmatrix} H_{11} & H_{12} & H_{13} \\ H_{21} & H_{22} & H_{23} \\ H_{31} & H_{32} & \bar{C}_2 \end{pmatrix} \tag{3}$$

where the elements of matrix $H(\theta, \dot{\theta})$ are [5]

$$\begin{aligned} H_{11} = {} & m_1 r_1^2 \dot{\theta}_1 sin(2\theta_1) + 2m_2 l_1^2 \dot{\theta}_1 cos(\theta_1) sin(\theta_1) + \\ & + 2m_2 r_2^2 \dot{\theta}_1 cos(\theta_1 + \theta_2) sin(\theta_1 + \theta_2) + \\ & + 2m_2 r_2^2 \dot{\theta}_0 cos(\theta_1 + \theta_2) sin(\theta_1 + \theta_2) + \\ & + 2m_2 l_1 r_2 \dot{\theta}_1 cos(\theta_1) sin(\theta_1 + \theta_2) + \\ & + 2m_2 l_1 r_2 \dot{\theta}_1 cos(\theta_1 + \theta_2) sin(\theta_1) + \\ & + 2m_2 l_1 r_2 \dot{\theta}_2 cos(\theta_1 + \theta_2) sin(\theta_1) + \bar{C}_0 \end{aligned} \tag{4}$$

$$H_{12} = -m_1 l_0 r_1 \dot{\theta}_1 sin(\theta_1) - m_2 l_0 l_1 \dot{\theta}_1 sin(\theta_1) - m_2 l_0 r_2 \dot{\theta}_1 sin(\theta_1 + \theta_2) \tag{5}$$

$$H_{13} = -2m_{12} l_0 r_2 \dot{\theta}_1 sin(\theta_1 + \theta_2) - m_2 l_0 r_2 \dot{\theta}_2 sin(\theta_1 + \theta_2) \tag{6}$$

$$\begin{gathered} H_{21} = -\tfrac{1}{2} m_1 r_1^2 \dot{\theta}_0 sin(2\theta_1) - 2m_1 r_2^2 \dot{\theta_0} sin(2(\theta_1 + \theta_2)) - \\ -m_2 l_1^2 \dot{\theta}_0 cos(\theta_1) sin(\theta_1) - m_2 l_1 r_2 \dot{\theta}_0 sin(2\theta_1 + \theta_2) \end{gathered} \tag{7}$$

$$H_{22} = -2m_2 l_1 r_2 \dot{\theta}_2 sin(\theta_2) + \bar{C}_1 \tag{8}$$

$$H_{23} = -m_2 l_1 r_2 \dot{\theta}_2 sin(\theta_2) \tag{9}$$

$$H_{31} = -\tfrac{1}{2} m_2 r_2^2 \dot{\theta}_0 sin(2(\theta_1 + \theta_2)) - m_2 l_1 r_2 \dot{\theta}_0 sin(\theta_1) cos(\theta_1 + \theta_2) \tag{10}$$

$$H_{32} = m_2 l_1 r_2 \dot{\theta}_1 sin(\theta_2) \tag{11}$$

In particular, about the elements of the Coriolis forces vector it holds that

$$C(\theta, \dot{\theta}) = \begin{pmatrix} H_{11} & H_{12} & H_{13} \\ H_{21} & H_{22} & H_{23} \\ H_{31} & H_{32} & C_2 \end{pmatrix} \begin{pmatrix} \dot{\theta}_1 \\ \dot{\theta}_2 \\ \dot{\theta}_3 \end{pmatrix} \Rightarrow C(\theta, \dot{\theta}) = \begin{pmatrix} H_{11}\dot{\theta}_1 + H_{12}\dot{\theta}_2 + H_{13}\dot{\theta}_3 \\ H_{21}\dot{\theta}_1 + H_{22}\dot{\theta}_2 + H_{23}\dot{\theta}_3 \\ H_{31}\dot{\theta}_1 + H_{32}\dot{\theta}_2 + H_{33}\dot{\theta}_3 \end{pmatrix} \tag{12}$$

In the previous equations m_0, m_1, m_2 are the masses of the links, and J_0, J_1, J_2 are moments of inertia. Besides, l_0, l_1, l_2 are the lengths of the links and r_0, r_1, r_2 are the distance between the bases of the links and their centers of gravity. Moreover, $\bar{C}_0$, $\bar{C}_1$, $\bar{C}_2$ are constants. About the gravitational forces vector one has [5]

$$G(\theta) = \begin{pmatrix} 0 & g_2(\theta) & g_3(\theta) \end{pmatrix}^T \tag{13}$$

where the elements of the gravitational forces vector are $g_2(\theta) = -g((m_1 r_1 + m_2 l_1) sin(\theta_1) + m_2 r_2 sin(\theta_1 + \theta_2))$ and $g_3(\theta) = -m_2 g r_2 sin(\theta_1 + \theta_2)$. Consequently, the dynamic model of the rotary double inverted pendulum is written as

$$\begin{gathered} M(\theta)\ddot{\theta} + H(\theta, \dot{\theta})\dot{\theta} + G(\theta) = \tau \Rightarrow \\ \ddot{\theta} = -M^{-1}(\theta)[C(\theta, \dot{\theta}) + G(\theta)] + M^{-1}(\theta)\tau \end{gathered} \tag{14}$$

The inverse of the inertia matrix $M(\theta)$ is denoted as

$$M(\theta)^{-1} = \tfrac{1}{detM} \begin{pmatrix} M_{11} & -M_{21} & M_{31} \\ -M_{12} & M_{22} & -M_{32} \\ M_{13} & -M_{23} & M_{33} \end{pmatrix} \tag{15}$$

where the sub-determinants M_{ij} $i = 1, 2, 3$ $j = 1, 2, 3$ are defined as: $M_{11} = m_{22}m_{33} - m_{32}m_{23}$, $M_{12} = m_{21}m_{33} - m_{31}m_{23}$, $M_{13} = m_{21}m_{32} - m_{31}m_{22}$, $M_{21} = m_{12}m_{33} - m_{32}m_{13}$, $M_{22} = m_{11}m_{33} - m_{31}m_{13}$, $M_{23} = m_{11}m_{32} - m_{31}m_{12}$, $M_{23} = m_{11}m_{32} - m_{31}m_{12}$, $M_{31} = m_{12}m_{23} - m_{22}m_{13}$, $M_{32} = m_{11}m_{23} - m_{21}m_{13}$, $M_{33} = m_{11}m_{22} - m_{21}m_{12}$ and $detM = m_1 M_{11} - m_{12}M_{12} + m_{13}M_{13}$.

Using Eq. (14) and Eq. (15) the dynamic model of the rotary double inverted pendulum becomes

$$\begin{pmatrix}\ddot{\theta}_0\\ \ddot{\theta}_1\\ \ddot{\theta}_2\end{pmatrix}=-\frac{1}{detM}\begin{pmatrix}M_{11} & -M_{21} & M_{31}\\ -M_{12} & M_{22} & -M_{32}\\ M_{13} & -M_{23} & M_{33}\end{pmatrix}\begin{pmatrix}C_1(\theta,\dot{\theta})+G_1(\theta)\\ C_2(\theta,\dot{\theta})+G_2(\theta)\\ C_3(\theta,\dot{\theta})+G_3(\theta)\end{pmatrix}+\frac{1}{detM}\begin{pmatrix}M_{11} & -M_{21} & M_{31}\\ -M_{12} & M_{22} & -M_{32}\\ M_{13} & -M_{23} & M_{33}\end{pmatrix}\begin{pmatrix}T_1\\ 0\\ 0\end{pmatrix} \tag{16}$$

or equivalently

$$\begin{pmatrix}\ddot{\theta}_0\\ \ddot{\theta}_1\\ \ddot{\theta}_2\end{pmatrix}=\begin{pmatrix}\frac{-M_{11}(C_1(\theta,\dot{\theta})+G_1(\theta))+M_{21}(C_2(\theta,\dot{\theta})+G_2(\theta))-M_{31}(C_3(\theta,\dot{\theta})+G_3(\theta))}{detM}\\ \frac{M_{12}(C_1(\theta,\dot{\theta})+G_1(\theta))-M_{22}(C_2(\theta,\dot{\theta})+G_2(\theta))+M_{32}(C_3(\theta,\dot{\theta})+G_3(\theta))}{detM}\\ \frac{-M_{13}(C_1(\theta,\dot{\theta})+G_1(\theta))+M_{23}(C_2(\theta,\dot{\theta})+G_2(\theta))-M_{33}(C_3(\theta,\dot{\theta})+G_3(\theta))}{detM}\end{pmatrix}+\begin{pmatrix}\frac{M_{11}}{detM}\\ -\frac{M_{12}}{detM}\\ \frac{M_{13}}{detM}\end{pmatrix}T_1 \tag{17}$$

Next, by denoting the state vector of the rotary double inverted pendulum as $x=[x_1,x_2,x_3,x_4,x_5,x_6]^T$ that is $x=[\theta_0,\dot{\theta}_0,\theta_1,\dot{\theta}_1,\theta_2,\dot{\theta}_2]^T$ and the control inputs vector as $u=T_1$ one has the state-space description

$$\begin{pmatrix}\dot{x}_1\\ \dot{x}_2\\ \dot{x}_3\\ \dot{x}_4\\ \dot{x}_5\\ \dot{x}_6\end{pmatrix}=\begin{pmatrix}x_2\\ f_2(x)\\ x_4\\ f_4(x)\\ x_6\\ f_6(x)\end{pmatrix}+\begin{pmatrix}0\\ g_2(x)\\ 0\\ g_4(x)\\ 0\\ g_6(x)\end{pmatrix}u \tag{18}$$

which is a model in the nonlinear affine-in-the-input state-space form

$$\dot{x}=f(x)+g(x)u \tag{19}$$

with $x\in R^{6\times 1}$, $f(x)\in R^{6\times 1}$, $g(x)\in R^{6\times 1}$, and $u\in R$. About the elements of vectors $f(x)$ and $g(x)$ which appear in this state-space model it holds that:

$$\begin{array}{cc} f_1(x)=x_2 & g_1(x)=0\\ f_2(x)=\frac{-M_{11}(C_1(\theta,\dot{\theta})+G_1(\theta))+M_{21}(C_2(\theta,\dot{\theta})+G_2(\theta))-M_{31}(C_3(\theta,\dot{\theta})+G_3(\theta))}{detM} & g_2(x)=\frac{M_{11}}{detM}\\ f_3(x)=x_4 & g_3(x)=0\\ f_4(x)=\frac{M_{12}(C_1(\theta,\dot{\theta})+G_1(\theta))-M_{22}(C_2(\theta,\dot{\theta})+G_2(\theta))+M_{32}(C_3(\theta,\dot{\theta})+G_3(\theta))}{detM} & g_4(x)=-\frac{M_{12}}{detM}\\ f_5(x)=x_6 & g_5(x)=0\\ f_6(x)=\frac{-M_{13}(C_1(\theta,\dot{\theta})+G_1(\theta))+M_{23}(C_2(\theta,\dot{\theta})+G_2(\theta))-M_{33}(C_3(\theta,\dot{\theta})+G_3(\theta))}{detM} & g_6(x)=\frac{M_{13}}{detM}\end{array} \tag{20}$$

3 Approximate linearization of the rotary double inverted pendulum

3.1 Linearization process

The dynamic model of the rotary double inverted pendulum undergoes approximate linearization around the temporary operating point (x^*,u^*) at each sampling instance [2-4]. This operating point is defined by x^* which is the value of the state vector at the present sampling instance and by u^* which is the last sampled value of the control inputs vector. The linearization process is based on first-order Taylor series expansion and on the computation of the associated Jacobian matrices. It brings the system from the initial nonlinear state-space form:

$$\dot{x}=f(x)+g(x)u \tag{21}$$

into the equivalent linearized state-space description

$$\dot{x} = Ax + Bu + \tilde{d} \tag{22}$$

where $\tilde{d}$ is the cumulative vector of disturbances which may incorporate (i) modelling errors due to the truncation of higher-order terms from the Taylor series expansion, (ii) exogenous perturbations, (iii) sensor measurement noise of any distribution. The disturbances' effects will be compensated by the robustness of the nonlinear optimal (H-infinity) control algorithm. The computation of the Jacobian matrices of the system is as follows:

$$A = \nabla_x[f(x) + g(x)u] \mid_{(x^*,u^*)} \Rightarrow A = \nabla_x[f(x)] \mid_{(x^*,u^*)} + \nabla_x[g(x)]u \mid_{(x^*,u^*)} \tag{23}$$

$$B = \nabla_u[f(x) + g(x)u] \mid_{(x^*,u^*)} \Rightarrow B = g(x) \mid_{(x^*,u^*)} \tag{24}$$

This linearization approach which has been followed for implementing the nonlinear optimal control scheme results into a quite accurate model of the system's dynamics. Consider for instance the following affine-in-the-input state-space model

$$\begin{gathered}\dot{x} = f(x) + g(x)u \Rightarrow \\ \dot{x} = [f(x^*) + \nabla_x f(x) \mid_{x^*} (x - x^*)] + [g(x^*) + \nabla_x g(x) \mid_{x^*} (x - x^*)]u^* + g(x^*)u^* + g(x^*)(u - u^*) + \tilde{d}_1 \Rightarrow \\ \dot{x} = [\nabla_x f(x) \mid_{x^*} + \nabla_x g(x) \mid_{x^*} u^*]x + g(x^*)u - [\nabla_x f(x) \mid_{x^*} + \nabla_x g(x) \mid_{x^*} u^*]x^* + f(x^*) + g(x^*)u^* + \tilde{d}_1\end{gathered} \tag{25}$$

where $\tilde{d}_1$ is the modelling error due to truncation of higher order terms in the Taylor series expansion of $f(x)$ and $g(x)$. Next, by defining $A = [\nabla_x f(x) \mid_{x^*} + \nabla_x g(x) \mid_{x^*} u^*]$, $B = g(x^*)$ one obtains

$$\dot{x} = Ax + Bu - Ax^* + f(x^*) + g(x^*)u^* + \tilde{d}_1 \tag{26}$$

Moreover by denoting $\tilde{d} = -Ax^* + f(x^*) + g(x^*)u^* + \tilde{d}_1$ about the cumulative modelling error term in the Taylor series expansion procedure one has

$$\dot{x} = Ax + Bu + \tilde{d} \tag{27}$$

which is the approximately linearized model of the dynamics of the system of Eq. (22). The term $f(x^*) + g(x^*)u^*$ is the derivative of the state vector at (x^*, u^*) which is almost annihilated by $-Ax^*$.

3.2 Computation of Jacobian matrices

Computation of the elements of the Jacobian matrix $\nabla_x[f(x)] \mid_{(x^*,u^*)}$ is first carried out.

First row of the Jacobian matrix $\nabla_x[f(x)] \mid_{(x^*,u^*)}$: $\frac{\partial f_1(x)}{\partial x_1} = 0$, $\frac{\partial f_1(x)}{\partial x_2} = 1$, $\frac{\partial f_1(x)}{\partial x_3} = 0$, $\frac{\partial f_1(x)}{\partial x_4} = 0$, $\frac{\partial f_1(x)}{\partial x_5} = 0$ and $\frac{\partial f_1(x)}{\partial x_6} = 0$.

Second row of the Jacobian matrix $\nabla_x[f(x)] \mid_{(x^*,u^*)}$: It holds that $f_2(x) = \frac{f_{2,num}(x)}{f_{2,den}(x)}$ where $f_{2,num}(x) = -M_{11}(C_1(\theta, \dot{\theta}) + G_1(\theta)) + M_{21}(C_2)(\theta, \dot{\theta} + G_2(\theta)) - M_{31}(C_3(\theta, \dot{\theta}) + G_3(\theta))$ and $f_{2,den}(x) = detM$. Moreover, one has that for $i = 1, 2, \cdots, 6$

$$\frac{\partial f_2(x)}{\partial x_i} = \frac{\frac{\partial f_{2,num}(x)}{\partial x_i} f_{2,den}(x) - f_{2,num}(x)\frac{\partial f_{2,den}(x)}{\partial x_i}}{f_{2,den}(x)^2} \tag{28}$$

Moreover, it holds that for $i = 1, 2, \cdots, 6$

$$\frac{\partial f_{2,num}(x)}{\partial x_i} = -\frac{\partial M_{11}}{\partial x_i}(C_1(\theta,\dot{\theta}) + G_1(\theta)) - M_{11}(\frac{\partial C_1(\theta,\dot{\theta})}{\partial x_i} + \frac{\partial G_1(\theta)}{\partial x_i}) + \\ + \frac{\partial M_{21}}{\partial x_i}(C_2(\theta,\dot{\theta}) + G_2(\theta)) + M_{21}(\frac{\partial C_2(\theta,\dot{\theta})}{\partial x_i} + \frac{\partial G_2(\theta)}{\partial x_i}) - \\ - \frac{\partial M_{31}}{\partial x_i}(C_3(\theta,\dot{\theta}) + G_3(\theta)) - M_{31}(\frac{\partial C_3(\theta,\dot{\theta})}{\partial x_i} + \frac{\partial G_3(\theta)}{\partial x_i}) \tag{29}$$

$$\frac{\partial f_{2,den}(x)}{\partial x_i} = \frac{\partial detM}{\partial x_i} \tag{30}$$

Third row of the Jacobian matrix $\nabla_x[f(x)] \mid_{(x^*,u^*)}$: $\frac{\partial f_3(x)}{\partial x_1} = 0$, $\frac{\partial f_3(x)}{\partial x_2} = 0$, $\frac{\partial f_3(x)}{\partial x_3} = 0$, $\frac{\partial f_3(x)}{\partial x_4} = 1$, $\frac{\partial f_3(x)}{\partial x_5} = 0$ and $\frac{\partial f_3(x)}{\partial x_6} = 0$.

Fourth row of the Jacobian matrix $\nabla_x[f(x)] \mid_{(x^*,u^*)}$: It holds that $f_4(x) = \frac{f_{4,num}(x)}{f_{4,den}(x)}$ where $f_{4,num}(x) = M_{12}(C_1(\theta,\dot{\theta}) + G_1(\theta)) - M_{22}(C_2)(\theta,\dot{\theta} + G_2(\theta)) + M_{32}(C_3(\theta,\dot{\theta}) + G_3(\theta))$ and $f_{4,den}(x) = detM$. Moreover, one has that for $i = 1, 2, \cdots, 6$

$$\frac{\partial f_4(x)}{\partial x_i} = \frac{\frac{\partial f_{4,num}(x)}{\partial x_i} f_{4,den}(x) - f_{4,num}(x)\frac{\partial f_{4,den}(x)}{\partial x_i}}{f_{4,den}(x)^2} \tag{31}$$

Moreover, it holds that for $i = 1, 2, \cdots, 6$

$$\frac{\partial f_{4,num}(x)}{\partial x_i} = \frac{\partial M_{12}}{\partial x_i}(C_1(\theta,\dot{\theta}) + G_1(\theta)) + M_{13}(\frac{\partial C_1(\theta,\dot{\theta})}{\partial x_i} + \frac{\partial G_1(\theta)}{\partial x_i}) - \\ - \frac{\partial M_{22}}{\partial x_i}(C_2(\theta,\dot{\theta}) + G_2(\theta)) - M_{22}(\frac{\partial C_2(\theta,\dot{\theta})}{\partial x_i} + \frac{\partial G_2(\theta)}{\partial x_i}) + \\ + \frac{\partial M_{32}}{\partial x_i}(C_3(\theta,\dot{\theta}) + G_3(\theta)) + M_{32}(\frac{\partial C_3(\theta,\dot{\theta})}{\partial x_i} + \frac{\partial G_3(\theta)}{\partial x_i}) \tag{32}$$

$$\frac{\partial f_{4,den}(x)}{\partial x_i} = \frac{\partial detM}{\partial x_i} \tag{33}$$

Fifth row of the Jacobian matrix $\nabla_x[f(x)] \mid_{(x^*,u^*)}$: $\frac{\partial f_5(x)}{\partial x_1} = 0$, $\frac{\partial f_5(x)}{\partial x_2} = 0$, $\frac{\partial f_5(x)}{\partial x_3} = 0$, $\frac{\partial f_5(x)}{\partial x_4} = 0$, $\frac{\partial f_5(x)}{\partial x_5} = 0$ and $\frac{\partial f_5(x)}{\partial x_6} = 0$.

Sixth row of the Jacobian matrix $\nabla_x[f(x)] \mid_{(x^*,u^*)}$: It holds that $f_6(x) = \frac{f_{6,num}(x)}{f_{6,den}(x)}$ where $f_{6,num}(x) = -M_{13}(C_1(\theta,\dot{\theta}) + G_1(\theta)) + M_{23}(C_2)(\theta,\dot{\theta} + G_2(\theta)) - M_{33}(C_3(\theta,\dot{\theta}) + G_3(\theta))$ and $f_{6,den}(x) = detM$. Moreover, one has that for $i = 1, 2, \cdots, 6$

$$\frac{\partial f_6(x)}{\partial x_i} = \frac{\frac{\partial f_{6,num}(x)}{\partial x_i} f_{6,den}(x) - f_{6,num}(x)\frac{\partial f_{6,den}(x)}{\partial x_i}}{f_{6,den}(x)^2} \tag{34}$$

Moreover, it holds that for $i = 1, 2, \cdots, 6$

$$\frac{\partial f_{6,num}(x)}{\partial x_i} = -\frac{\partial M_{13}}{\partial x_i}(C_1(\theta,\dot{\theta}) + G_1(\theta)) - M_{13}(\frac{\partial C_1(\theta,\dot{\theta})}{\partial x_i} + \frac{\partial G_1(\theta)}{\partial x_i}) + \\ + \frac{\partial M_{23}}{\partial x_i}(C_2(\theta,\dot{\theta}) + G_2(\theta)) + M_{23}(\frac{\partial C_2(\theta,\dot{\theta})}{\partial x_i} + \frac{\partial G_2(\theta)}{\partial x_i}) - \\ - \frac{\partial M_{33}}{\partial x_i}(C_3(\theta,\dot{\theta}) + G_3(\theta)) - M_{33}(\frac{\partial C_3(\theta,\dot{\theta})}{\partial x_i} + \frac{\partial G_3(\theta)}{\partial x_i}) \tag{35}$$

$$\frac{\partial f_{6,den}(x)}{\partial x_i} = \frac{\partial detM}{\partial x_i} \tag{36}$$

Computation of the elements of the Jacobian matrix $\nabla_x[g(x)] \mid_{(x^*,u^*)}$ is also carried out.

First row of the Jacobian matrix $\nabla_x[g(x)] \mid_{(x^*,u^*)}$: $\frac{\partial g_1(x)}{\partial x_i} = 0$ for $i = 1, 2, \cdots, 6$.

Second row of the Jacobian matrix $\nabla_x[g(x)] \mid_{(x^*,u^*)}$: It holds that for $i = 1, 2, \cdots, 6$

$$\frac{\partial g_{21}}{\partial x_i} = \frac{\frac{dM_{11}}{dx_i} detM - M_{11}\frac{ddetM}{dx_i}}{detM^2} \tag{37}$$

Third row of the Jacobian matrix $\nabla_x[g(x)]\mid_{(x^*,u^*)}$: $\frac{\partial g_3(x)}{\partial x_i}=0$ for $i=1,2,\cdots,6$.

Fourth row of the Jacobian matrix $\nabla_x[g(x)]\mid_{(x^*,u^*)}$: It holds that for $i=1,2,\cdots,6$

$$\frac{\partial g_{41}}{\partial x_i}=\frac{-\frac{dM_{12}}{dx_i}detM+M_{11}\frac{ddetM}{dx_i}}{detM^2} \tag{38}$$

Fifth row of the Jacobian matrix $\nabla_x[g(x)]\mid_{(x^*,u^*)}$: $\frac{\partial g_3(x)}{\partial x_i}=0$ for $i=1,2,\cdots,6$.

Sixth row of the Jacobian matrix $\nabla_x[g(x)]\mid_{(x^*,u^*)}$: It holds that for $i=1,2,\cdots,6$

$$\frac{\partial g_{61}}{\partial x_i}=\frac{\frac{dM_{13}}{dx_i}detM-M_{13}\frac{ddetM}{dx_i}}{detM^2} \tag{39}$$

Besides, the partial derivatives of the sub-determinants of the inertial matrix M are computed as follows: For $i=1,2,\cdots,6$

$$\frac{\partial M_{11}}{\partial x_i}=\frac{\partial m_{22}}{\partial x_i}m_{33}+m_{22}\frac{\partial m_{33}}{\partial x_i}-\frac{\partial m_{32}}{\partial x_i}m_{23}-m_{32}\frac{\partial m_{23}}{\partial x_i} \tag{40}$$

$$\frac{\partial M_{12}}{\partial x_i}=\frac{\partial m_{21}}{\partial x_i}m_{33}+m_{21}\frac{\partial m_{33}}{\partial x_i}-\frac{\partial m_{31}}{\partial x_i}m_{23}-m_{31}\frac{\partial m_{23}}{\partial x_i} \tag{41}$$

$$\frac{\partial M_{13}}{\partial x_i}=\frac{\partial m_{21}}{\partial x_i}m_{32}+m_{21}\frac{\partial m_{32}}{\partial x_i}-\frac{\partial m_{31}}{\partial x_i}m_{22}-m_{31}\frac{\partial m_{22}}{\partial x_i} \tag{42}$$

$$\frac{\partial M_{21}}{\partial x_i}=\frac{\partial m_{12}}{\partial x_i}m_{33}+m_{12}\frac{\partial m_{33}}{\partial x_i}-\frac{\partial m_{32}}{\partial x_i}m_{13}-m_{32}\frac{\partial m_{13}}{\partial x_i} \tag{43}$$

$$\frac{\partial M_{22}}{\partial x_i}=\frac{\partial m_{11}}{\partial x_i}m_{33}+m_{11}\frac{\partial m_{33}}{\partial x_i}-\frac{\partial m_{31}}{\partial x_i}m_{13}-m_{31}\frac{\partial m_{13}}{\partial x_i} \tag{44}$$

$$\frac{\partial M_{23}}{\partial x_i}=\frac{\partial m_{11}}{\partial x_i}m_{32}+m_{11}\frac{\partial m_{32}}{\partial x_i}-\frac{\partial m_{31}}{\partial x_i}m_{13}-m_{31}\frac{\partial m_{13}}{\partial x_i} \tag{45}$$

$$\frac{\partial M_{31}}{\partial x_i}=\frac{\partial m_{12}}{\partial x_i}m_{23}+m_{12}\frac{\partial m_{23}}{\partial x_i}-\frac{\partial m_{22}}{\partial x_i}m_{13}-m_{22}\frac{\partial m_{13}}{\partial x_i} \tag{46}$$

$$\frac{\partial M_{32}}{\partial x_i}=\frac{\partial m_{11}}{\partial x_i}m_{23}+m_{11}\frac{\partial m_{23}}{\partial x_i}-\frac{\partial m_{21}}{\partial x_i}m_{13}-m_{21}\frac{\partial m_{13}}{\partial x_i} \tag{47}$$

$$\frac{\partial M_{33}}{\partial x_i}=\frac{\partial m_{11}}{\partial x_i}m_{22}+m_{11}\frac{\partial m_{22}}{\partial x_i}-\frac{\partial m_{21}}{\partial x_i}m_{12}-m_{21}\frac{\partial m_{12}}{\partial x_i} \tag{48}$$

About the partial derivative of the determinant of the inertia matrix M it holds that

$$\begin{array}{c}\frac{\partial detM}{\partial x_i}=\frac{\partial m_{11}}{\partial x_i}M_{11}+m_{11}\frac{\partial M_{11}}{\partial x_i}-\\ -\frac{\partial m_{12}}{\partial x_i}M_{12}+m_{12}\frac{\partial M_{12}}{\partial x_i}+\\ +\frac{\partial m_{13}}{\partial x_i}M_{13}+m_{13}\frac{\partial M_{13}}{\partial x_i}\end{array} \tag{49}$$

Moreover, about the partial derivatives m_{ij}, $i=1,2,3$ and $j=1,2,3$ which appear in the inertia matrix it holds that:

$\frac{\partial m_{11}}{\partial x_1}=0$, $\frac{\partial m_{11}}{\partial x_2}=0$, $\frac{\partial m_{11}}{\partial x_3}=(m_1r_1^2+m_2l_2^2)2sin(x_3)cos(x_3)+2m_2l_1r_2[cos(x_3)sin(x_3+x_5)+sin(x_3)cos(x_3+x_5)]+m_2r_3^2 2sin(x_3+x_5)cos(x_3+x_5)$, $\frac{\partial m_{11}}{\partial x_4}=0$, $\frac{\partial m_{11}}{\partial x_5}=2m_2l_1r_2sin(x_3)cos(x_3+x_5)+m_2r_2^2 2sin(x_3+x_5)cos(x_3+x_5)$, $\frac{\partial m_{11}}{\partial x_6}=0$.

$\frac{\partial m_{12}}{\partial x_1}=0$, $\frac{\partial m_{12}}{\partial x_2}=0$, $\frac{\partial m_{12}}{\partial x_3}=-m_1l_0r_1sin(x_3)-m_2l_0r_2sin(x_3+x_5)-m_2l_0l_1sin(x_3)$, $\frac{\partial m_{12}}{\partial x_4}=0$, $\frac{\partial m_{12}}{\partial x_5}=-m_2l_0r_2sin(x_3+x_5)$, $\frac{\partial m_{12}}{\partial x_6}=0$.

$\frac{\partial m_{13}}{\partial x_1}=0$, $\frac{\partial m_{13}}{\partial x_2}=0$, $\frac{\partial m_{13}}{\partial x_3}=-m_21l_0r_2sin(x_3+x_5)$, $\frac{\partial m_{13}}{\partial x_4}=0$, $\frac{\partial m_{13}}{\partial x_5}=-m_2l_0r_2sin(x_3+x_5)$, $\frac{\partial m_{13}}{\partial x_6}=0$.

$\frac{\partial m_{21}}{\partial x_1}=0$, $\frac{\partial m_{21}}{\partial x_2}=0$, $\frac{\partial m_{21}}{\partial x_3}=-m_1l_0r_1sin(x_3)-m_2l_0r_2sin(x_3+x_5)-m_2l_0l_1sin(x_3)$, $\frac{\partial m_{21}}{\partial x_4}=0$, $\frac{\partial m_{21}}{\partial x_5}=-m_2l_0r_2sin(x_3+x_5)$, $\frac{\partial m_{21}}{\partial x_6}=0$.

$\frac{\partial m_{22}}{\partial x_1}=0$, $\frac{\partial m_{22}}{\partial x_2}=0$, $\frac{\partial m_{22}}{\partial x_3}=0$, $\frac{\partial m_{22}}{\partial x_4}=0$, $\frac{\partial m_{22}}{\partial x_5}=-m_2l_1r_2sin(x_5)$, $\frac{\partial m_{22}}{\partial x_6}=0$.

$\frac{\partial m_{23}}{\partial x_1}=0$, $\frac{\partial m_{23}}{\partial x_2}=0$, $\frac{\partial m_{23}}{\partial x_3}=0$, $\frac{\partial m_{23}}{\partial x_4}=0$, $\frac{\partial m_{23}}{\partial x_5}=-m_2l_1r_2sin(x_5)$, $\frac{\partial m_{23}}{\partial x_6}=0$.

$\frac{\partial m_{31}}{\partial x_1}=0$, $\frac{\partial m_{31}}{\partial x_2}=0$, $\frac{\partial m_{31}}{\partial x_3}=-m_21l_0r_2sin(x_3+x_5)$, $\frac{\partial m_{31}}{\partial x_4}=0$, $\frac{\partial m_{31}}{\partial x_5}=-m_2l_0r_2sin(x_3+x_5)$, $\frac{\partial m_{31}}{\partial x_6}=0$.

$\frac{\partial m_{32}}{\partial x_1}=0$, $\frac{\partial m_{32}}{\partial x_2}=0$, $\frac{\partial m_{32}}{\partial x_3}=0$, $\frac{\partial m_{32}}{\partial x_4}=0$, $\frac{\partial m_{32}}{\partial x_5}=-m_2l_1r_2sin(x_5)$, $\frac{\partial m_{32}}{\partial x_6}=0$.

$\frac{\partial m_{33}}{\partial x_1}=0$, $\frac{\partial m_{33}}{\partial x_2}=0$, $\frac{\partial m_{33}}{\partial x_3}=0$, $\frac{\partial m_{33}}{\partial x_4}=0$, $\frac{\partial m_{33}}{\partial x_5}=0$, $\frac{\partial m_{33}}{\partial x_6}=0$.

Next, the partial derivatives of the elements of the Coriolis and centrifugal forces matrix $C(\theta,\dot{\theta})$ are computed. It holds that $C_1(\theta,\dot{\theta})=H_{11}x_2+H_{12}x_4+H_{13}x_6$, $C_2(\theta,\dot{\theta})=H_{21}x_2+H_{22}x_4+H_{23}x_6$, and $C_3(\theta,\dot{\theta})=H_{31}x_2+H_{32}x_4+H_{33}x_6$. Thus:

$\frac{\partial C_1}{\partial x_1}=\frac{\partial H_{11}}{\partial x_1}x_2+\frac{\partial H_{12}}{\partial x_1}x_4+\frac{\partial H_{13}}{\partial x_1}x_6$, $\frac{\partial C_1}{\partial x_2}=[\frac{\partial H_{11}}{\partial x_2}x_2+H_{11}]+\frac{\partial H_{12}}{\partial x_2}x_4+\frac{\partial H_{13}}{\partial x_2}x_6$, $\frac{\partial C_1}{\partial x_3}=\frac{\partial H_{11}}{\partial x_1}x_3+\frac{\partial H_{12}}{\partial x_3}x_4+\frac{\partial H_{13}}{\partial x_3}x_6$, $\frac{\partial C_1}{\partial x_4}=\frac{\partial H_{11}}{\partial x_4}x_2+[\frac{\partial H_{12}}{\partial x_4}x_4+H_{12}]+\frac{\partial H_{13}}{\partial x_4}x_6$, $\frac{\partial C_1}{\partial x_5}=\frac{\partial H_{11}}{\partial x_5}x_2+\frac{\partial H_{12}}{\partial x_5}x_4+\frac{\partial H_{13}}{\partial x_5}x_6$, $\frac{\partial C_1}{\partial x_6}=\frac{\partial H_{11}}{\partial x_6}x_2+\frac{\partial H_{12}}{\partial x_6}x_4+[\frac{\partial H_{13}}{\partial x_1}x_6+H_{13}]$.

$\frac{\partial C_2}{\partial x_1}=\frac{\partial H_{21}}{\partial x_1}x_2+\frac{\partial H_{22}}{\partial x_1}x_4+\frac{\partial H_{23}}{\partial x_1}x_6$, $\frac{\partial C_2}{\partial x_2}=[\frac{\partial H_{21}}{\partial x_2}x_2+H_{21}]+\frac{\partial H_{22}}{\partial x_2}x_4+\frac{\partial H_{23}}{\partial x_2}x_6$, $\frac{\partial C_2}{\partial x_3}=\frac{\partial H_{21}}{\partial x_1}x_3+\frac{\partial H_{22}}{\partial x_3}x_4+\frac{\partial H_{23}}{\partial x_3}x_6$, $\frac{\partial C_2}{\partial x_4}=\frac{\partial H_{21}}{\partial x_4}x_2+[\frac{\partial H_{22}}{\partial x_4}x_4+H_{22}]+\frac{\partial H_{23}}{\partial x_4}x_6$, $\frac{\partial C_2}{\partial x_5}=\frac{\partial H_{21}}{\partial x_5}x_2+\frac{\partial H_{22}}{\partial x_5}x_4+\frac{\partial H_{23}}{\partial x_5}x_6$, $\frac{\partial C_2}{\partial x_6}=\frac{\partial H_{21}}{\partial x_6}x_2+\frac{\partial H_{22}}{\partial x_6}x_4+[\frac{\partial H_{23}}{\partial x_1}x_6+H_{23}]$.

$\frac{\partial C_3}{\partial x_1}=\frac{\partial H_{31}}{\partial x_1}x_2+\frac{\partial H_{32}}{\partial x_1}x_4+\frac{\partial H_{33}}{\partial x_1}x_6$, $\frac{\partial C_3}{\partial x_2}=[\frac{\partial H_{31}}{\partial x_2}x_2+H_{31}]+\frac{\partial H_{32}}{\partial x_2}x_4+\frac{\partial H_{33}}{\partial x_2}x_6$, $\frac{\partial C_3}{\partial x_3}=\frac{\partial H_{31}}{\partial x_1}x_3+\frac{\partial H_{32}}{\partial x_3}x_4+\frac{\partial H_{33}}{\partial x_3}x_6$, $\frac{\partial C_3}{\partial x_4}=\frac{\partial H_{31}}{\partial x_4}x_2+[\frac{\partial H_{32}}{\partial x_4}x_4+H_{32}]+\frac{\partial H_{33}}{\partial x_4}x_6$, $\frac{\partial C_2}{\partial x_5}=\frac{\partial H_{21}}{\partial x_5}x_2+\frac{\partial H_{22}}{\partial x_5}x_4+\frac{\partial H_{23}}{\partial x_5}x_6$, $\frac{\partial C_3}{\partial x_6}=\frac{\partial H_{31}}{\partial x_6}x_2+\frac{\partial H_{32}}{\partial x_6}x_4+[\frac{\partial H_{33}}{\partial x_1}x_6+H_{33}]$.

About the partial derivatives of the terms H_{ij}, $i=1,2,3$ and $j=1,2,3$ one has that $\frac{\partial H_{11}}{\partial x_1}=0$, $\frac{\partial H_{11}}{\partial x_2}=0$

$$\begin{aligned}\frac{\partial H_{11}}{\partial x_3}=&m_1r_1^2x_4^2 2cos(2x_3)+2m_2l_1^2x_4[cos^2(x_3)-sin^2(x_3)]+\\&+2m_2r_2^2x_4[cos^2(x_3+x_5)-sin^2(x_3+x_5)]+\\&+2m_2r_2^2x_6cos(x_3+x_5)sin(x_3+x_5)+\\&+2m_2l_1r_2x_4[cos(x_3)cos(x_3+x_5)-sin(x_3)sin(x_3+x_5)]+\\&+2m_2l_1r_2x_4[cos(x_3)cos(x_3+x_5)-sin(x_3)sin(x_3+x_5)]+\\&+2m_2l_1r_2x_6[cos(x_3+x_5)cos(x_3)-sin(x_3+x_5)sin(x_3)]\end{aligned}\tag{50}$$

$$\begin{aligned}\frac{\partial H_{11}}{\partial x_4}=&m_1r_1^2 2x_4sin(2x_3)+2m_2l_1^2cos(x_3)sin(x_3)+\\&+2m_2r_2^2cos(x_3+x_5)sin(x_3+x_5)+\\&+2m_2l_1r_2cos(x_3)sin(x_3+x_5)+\\&+2m_2l_1r_2cos(x_3+x_5)sin(x_3)\end{aligned}\tag{51}$$

$$\begin{array}{c}\frac{\partial H_{11}}{\partial x_5} = 2m_2r_2^2x_4[cos^2(x_3+x_5) - sin^2(x_3+x_5)]+\\ +2m_2r_2^2x_6[cos^2(x_3+x_5) - sin^2(x_3+x_5)]+\\ +2m_3l_1r_2x_4cos(x_3)cos(x_3+x_5)+\\ -2m_2l_1r_2x_4sin(x_3+x_5)sin(x_3)+\\ -2m_2l_1r_2x_6sin(x_3+x_5)sin(x_3)\end{array} \tag{52}$$

$$\begin{array}{c}\frac{\partial H_{11}}{\partial x_6} = 2m_2r_2^2cos(x_3+x_5)sin(x_3+x_5)+\\ +2m_2l_1r_2x_6sin(x_3+x_5)sin(x_3)\end{array} \tag{53}$$

In an equivalent manner one finds $\frac{\partial H_{12}}{\partial x_1} = 0$, $\frac{\partial H_{12}}{\partial x_2} = 0$,

$$\frac{\partial H_{12}}{\partial x_3} = -m_1l_0r_1x_4cos(x_3) - m_2l_0l_1x_4cos(x_3) - m_2l_0r_2x_4cos(x_3+x_5) \tag{54}$$

$$\frac{\partial H_{12}}{\partial x_4} = -m_1l_0r_1sin(x_3) - m_2l_0l_1sin(x_3) - m_2l_0r_2sin(x_3++x_5) \tag{55}$$

$$\frac{\partial H_{12}}{\partial x_5} = -m_2l_0r_2x_4cos(x_3+x_5) \tag{56}$$

and also $\frac{\partial H_{12}}{\partial x_6} = 0$. In a similar manner one obtains $\frac{\partial H_{13}}{\partial x_1} = 0$, $\frac{\partial H_{13}}{\partial x_2} = 0$ and also

$$\frac{\partial H_{13}}{\partial x_3} = -2m_1l_0r_2x_4cos(x_3+x_5) - m_2l_0r_0x_6cos(x_3+x_5) \tag{57}$$

$$\frac{\partial H_{13}}{\partial x_4} = -2m_1l_0r_0sin(x_3+x_5) \tag{58}$$

$$\frac{\partial H_{13}}{\partial x_5} = -2m_1l_0r_2x_4cos(x_3+x_5) - m_2l_0r_2x_6cos(x_3+x_5) \tag{59}$$

$$\frac{\partial H_{13}}{\partial x_6} = -m_2l_0r_2sin(x_3+x_5) \tag{60}$$

Additionally, one computes $\frac{\partial H_{21}}{\partial x_1} = 0$ and also

$$\begin{array}{c}\frac{\partial H_{21}}{\partial x_2} = -\frac{1}{2}m_1r_1^2sin(2x_3) - \frac{1}{2}m_2r_2^2sin(2(x_3+x+5))-\\ -m_2l_1^2cos(x_3)sin(x_3) - m_2l_1r_2sin(2x_3+x_5)\end{array} \tag{61}$$

$$\begin{array}{c}\frac{\partial H_{21}}{\partial x_3} = -\frac{1}{2}m_1r_1^2x_22cos(2x_3) - \frac{1}{2}m_2r_2^2x_22cos(2(x_3+x_5))-\\ -m_2l_1^2x_2[cos^2(x_3) - sin^2(x_3)] - m_2l_1r_2x_2^2cos^2(2x_3+x_5)\end{array} \tag{62}$$

$$\frac{\partial H_{21}}{\partial x_5} = -\frac{1}{2}m_2r_2^2x_2^2cos(2(x_3+x_5)) - m_2l_1r_2x_2cos(2x_3+x_5) \tag{63}$$

while it also holds $\frac{\partial H_{21}}{\partial x_4} = 0$ and $\frac{\partial H_{21}}{\partial x_6} = 0$. Additionally, one finds $\frac{\partial H_{22}}{\partial x_1} = 0$, $\frac{\partial H_{22}}{\partial x_2} = 0$, $\frac{\partial H_{22}}{\partial x_3} = 0$, $\frac{\partial H_{22}}{\partial x_4} = 0$ while it also holds that

$$\frac{\partial H_{22}}{\partial x_4} = -2m_2l_1r_2x_6cos(x_5) \tag{64}$$

$$\frac{\partial H_{22}}{\partial x_5} = -2m_2l_1r_2x_6sin(x_5) \tag{65}$$

In a similar manner one obtains $\frac{\partial H_{23}}{\partial x_1} = 0$, $\frac{\partial H_{23}}{\partial x_2} = 0$, $\frac{\partial H_{23}}{\partial x_3} = 0$, $\frac{\partial H_{23}}{\partial x_4} = 0$, and also

$$\frac{\partial H_{23}}{\partial x_5} = -m_2l_1r_2x_6cos(x_5) \tag{66}$$

$$\frac{\partial H_{23}}{\partial x_6} = -m_2l_1e_2sin(x_5) \tag{67}$$

Additionally, one finds $\frac{\partial H_{31}}{\partial x_1} = 0$ and also

$$\frac{\partial H_{31}}{\partial x_2} = -\frac{1}{2} m_2 r_2^2 sin(2(x_3 + x_5)) - m_2 l_1 r_2 sin(x_3) cos(x_3 + x_5) \tag{68}$$

$$\begin{gathered} \frac{\partial H_{31}}{\partial x_3} = -\frac{1}{2} m_2 r_2^2 x_2 2cos(2(x_3 + x_5)) - \\ -m_2 l_1 r_2 x_2 [cos(x_3) cos(x_3 + x_5) - sin(x_3) sin(x_3 + x_5)] \end{gathered} \tag{69}$$

$$\begin{gathered} \frac{\partial H_{31}}{\partial x_5} = -\frac{1}{2} m_2 r_2^2 x_2 - 2cos(2(x_3 + x_5)) + \\ + m_2 l_1 r_2 x_2 2sin(x_3) sin(x_3 + x_5) \end{gathered} \tag{70}$$

while it also holds that $\frac{\partial H_{31}}{\partial x_4} = 0$ and $\frac{\partial H_{31}}{\partial x_6} = 0$. Equivalently, one obtains $\frac{\partial H_{32}}{\partial x_1} = 0$, $\frac{\partial H_{32}}{\partial x_2} = 0$, $\frac{\partial H_{32}}{\partial x_3} = 0$, $\frac{\partial H_{31}}{\partial x_6} = 0$ and also

$$\frac{\partial H_{32}}{\partial x_4} = m_2 l_1 r_2 sin(x_5) \tag{71}$$

$$\frac{\partial H_{32}}{\partial x_5} = m_2 l_1 r_2 x_4 cos(x_5) \tag{72}$$

Finally it holds that $\frac{\partial H_{32}}{\partial x_6} = 0$ for $i = 1, 2, \cdots, 6$.

Next, the partial derivatives of the elements of the gravitational forces vector are computed. About the first element of the gravitational forces vector it holds that $\frac{\partial g_1}{\partial x_i} = 0$ for $i = 1, 2, \cdots, 6$.

For the second element of the gravitational forces vector one has $\frac{\partial g_2}{\partial x_1} = 0$, $\frac{\partial g_2}{\partial x_2} = 0$, $\frac{\partial g_2}{\partial x_4} = 0$, $\frac{\partial g_2}{\partial x_6} = 0$, and also

$$\frac{\partial g_2}{\partial x_3} = -g(m_1 r_1 + m_2 l_1 cos(x_3) + m_2 r_2 cos(x_3 + x_5)) \tag{73}$$

For the third element of the gravitational forces vector one has $\frac{\partial g_3}{\partial x_1} = 0$, $\frac{\partial g_3}{\partial x_2} = 0$, $\frac{\partial g_3}{\partial x_4} = 0$, $\frac{\partial g_3}{\partial x_6} = 0$, and also

$$\frac{\partial g_3}{\partial x_3} = -g m_2 r_2 cos(x_3 + x_5) \tag{74}$$

$$\frac{\partial g_3}{\partial x_5} = -g m_2 r_2 cos(x_3 + x_5) \tag{75}$$

4 Design of an H-infinity nonlinear feedback controller

4.1 Equivalent linearized dynamics of the rotary double inverted pendulum

After linearization around its current operating point, the dynamic model for the rotary double inverted pendulum is written as [2-4]

$$\dot{x} = Ax + Bu + d_1 \tag{76}$$

Parameter d_1 stands for the linearization error in the rotary double inverted pendulum's model that was given previously in Eq. (22). The reference setpoints for the state vector of the aforementioned dynamic model are denoted by $\mathbf{x_d} = [x_1^d, \cdots, x_6^d]$. Tracking of this trajectory is achieved after applying the control input u^*. At every time instant the control input u^* is assumed to differ from the control input u appearing in Eq. (76) by an amount equal to Δu, that is $u^* = u + \Delta u$

$$\dot{x}_d = Ax_d + Bu^* + d_2 \tag{77}$$

The dynamics of the controlled system described in Eq. (76) can be also written as

$$\dot{x} = Ax + Bu + Bu^* - Bu^* + d_1 \tag{78}$$

and by denoting $d_3 = -Bu^* + d_1$ as an aggregate disturbance term one obtains

$$\dot{x} = Ax + Bu + Bu^* + d_3 \tag{79}$$

By subtracting Eq. (77) from Eq. (79) one has

$$\dot{x} - \dot{x}_d = A(x - x_d) + Bu + d_3 - d_2 \tag{80}$$

By denoting the tracking error as $e = x - x_d$ and the aggregate disturbance term as $\tilde{d} = d_3 - d_2$, the tracking error dynamics becomes

$$\dot{e} = Ae + Bu + \tilde{d} \tag{81}$$

The above linearized form of the rotary double inverted pendulum can be efficiently controlled after applying an H-infinity feedback control scheme.

4.2 The nonlinear H-infinity control

The initial nonlinear model of the rotary double inverted pendulum is in the form

$$\dot{x} = f(x, u) \quad x \in R^n, \; u \in R^m \tag{82}$$

Linearization of the model of the rotary double inverted pendulum is performed at each iteration of the control algorithm round its present operating point $(x^*, u^*) = (x(t), u(t - T_s))$. The linearized equivalent of the system is described by

$$\dot{x} = Ax + Bu + L\tilde{d} \quad x \in R^n, \; u \in R^m, \; \tilde{d} \in R^q \tag{83}$$

where matrices A and B are obtained from the computation of the previously defined Jacobians and vector $\tilde{d}$ denotes disturbance terms due to linearization errors. The problem of disturbance rejection for the linearized model that is described by

$$\begin{aligned} \dot{x} &= Ax + Bu + L\tilde{d} \\ y &= Cx \end{aligned} \tag{84}$$

where $x \in R^n$, $u \in R^m$, $\tilde{d} \in R^q$ and $y \in R^p$, cannot be handled efficiently if the classical LQR control scheme is applied. This is because of the existence of the perturbation term $\tilde{d}$. The disturbance term $\tilde{d}$ apart from modeling (parametric) uncertainty and external perturbation terms can also represent noise terms of any distribution.

In the H_∞ control approach, a feedback control scheme is designed for trajectory tracking by the system's state vector and simultaneous disturbance rejection, considering that the disturbance affects the system in the worst possible manner. The disturbances' effects are incorporated in the following quadratic cost function [2-4]:

$$J(t) = \tfrac{1}{2}\int_0^T [y^T(t)y(t) + ru^T(t)u(t) - \rho^2 \tilde{d}^T(t)\tilde{d}(t)]dt, \quad r, \rho > 0 \tag{85}$$

The significance of the negative sign in the cost function's term that is associated with the perturbation variable $\tilde{d}(t)$ is that the disturbance tries to maximize the cost function $J(t)$ while the control signal $u(t)$ tries to minimize it. The physical meaning of the relation given above is that the control signal and the

disturbances compete to each other within a min-max differential game. This problem of min-max optimization can be written as $min_u max_{\tilde{d}} J(u, \tilde{d})$.

The objective of the optimization procedure is to compute a control signal $u(t)$ which can compensate for the worst possible disturbance, that is externally imposed to the rotary double inverted pendulum. However, the solution to the min-max optimization problem is directly related to the value of the parameter ρ. This means that there is an upper bound in the disturbances magnitude that can be annihilated by the control signal.

4.3 Computation of the feedback control gains

For the linearized system given by Eq. (84) the cost function of Eq. (85) is defined, where the coefficient r determines the penalization of the control input and the weight coefficient ρ determines the reward of the disturbances' effects. It is assumed that (i) The energy that is transferred from the disturbances signal $\tilde{d}(t)$ is bounded, that is $\int_0^\infty \tilde{d}^T(t)\tilde{d}(t)dt < \infty$, (ii) matrices $[A, B]$ and $[A, L]$ are stabilizable, (iii) matrix $[A, C]$ is detectable. In the case of a tracking problem the optimal feedback control law is given by [2-4]

$$u(t) = -Ke(t) \tag{86}$$

with $e = x - x_d$ to be the tracking error, and $K = \frac{1}{r}B^T P$ where P is a positive definite symmetric matrix. As it will be proven in Section 5, matrix P is obtained from the solution of the Riccati equation [2-4]

$$A^T P + PA + Q - P(\tfrac{2}{r}BB^T - \tfrac{1}{\rho^2}LL^T)P = 0 \tag{87}$$

where Q is a positive semi-definite symmetric matrix. The worst case disturbance is given by

$$\tilde{d}(t) = \tfrac{1}{\rho^2}L^T P e(t) \tag{88}$$

The solution of the H-infinity feedback control problem for the rotary double inverted pendulum and the computation of the worst case disturbance that the related controller can sustain, comes from superposition of Bellman's optimality principle when considering that the rotary double inverted pendulum is affected by two separate inputs (i) the control input u (ii) the cumulative disturbance input $\tilde{d}(t)$. Solving the optimal control problem for u, that is for the minimum variation (optimal) control input that achieves elimination of the state vector's tracking error, gives $u = -\frac{1}{r}B^T P e$. Equivalently, solving the optimal control problem for $\tilde{d}$, that is for the worst case disturbance that the control loop can sustain gives $\tilde{d} = \frac{1}{\rho^2}L^T P e$.

The diagram of the considered control loop for the rotary double inverted pendulum is depicted in Fig. 2.

5 Lyapunov stability analysis

5.1 Stability proof

Through Lyapunov stability analysis it will be shown that the proposed nonlinear control scheme assures H_∞ tracking performance for the rotary double inverted pendulum, and that in case of bounded disturbance terms asymptotic convergence to the reference setpoints is achieved. The tracking error dynamics for the rotary double inverted pendulum is written in the form

$$\dot{e} = Ae + Bu + L\tilde{d} \tag{89}$$

where in the rotary double inverted pendulum's case $L = \in R^{6\times 6}$ to be the disturbance inputs gain matrix. Variable $\tilde{d}$ denotes model uncertainties and external disturbances of the rotary double inverted pendulum's model. The following Lyapunov equation is considered [2-4]

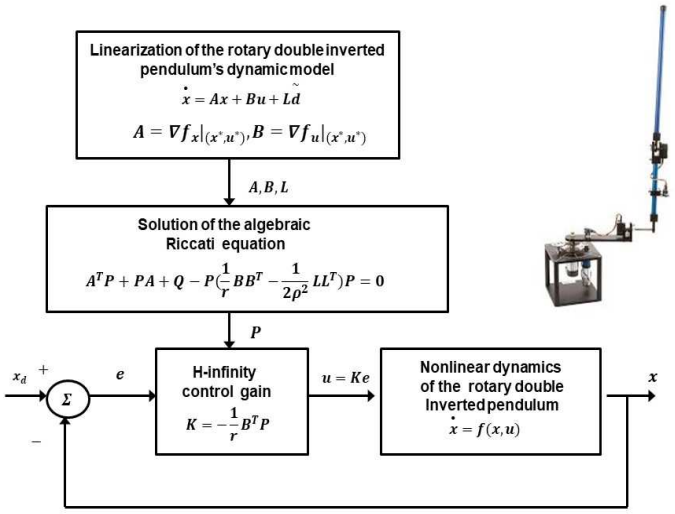

Figure 2: Diagram of the control scheme for the rotary double inverted pendulum

$$V = \tfrac{1}{2}e^TPe \tag{90}$$

where $e = x - x_d$ is the tracking error. By differentiating with respect to time one obtains

$$\dot{V} = \tfrac{1}{2}\dot{e}^TPe + \tfrac{1}{2}e^TP\dot{e} \Rightarrow \dot{V} = \tfrac{1}{2}[Ae + Bu + L\tilde{d}]^TPe + \tfrac{1}{2}e^TP[Ae + Bu + L\tilde{d}] \Rightarrow \tag{91}$$

$$\dot{V} = \tfrac{1}{2}[e^TA^T + u^TB^T + \tilde{d}^TL^T]Pe + \tfrac{1}{2}e^TP[Ae + Bu + L\tilde{d}] \Rightarrow \tag{92}$$

$$\dot{V} = \tfrac{1}{2}e^TA^TPe + \tfrac{1}{2}u^TB^TPe + \tfrac{1}{2}\tilde{d}^TL^TPe + \tfrac{1}{2}e^TPAe + \tfrac{1}{2}e^TPBu + \tfrac{1}{2}e^TPL\tilde{d} \tag{93}$$

The previous equation is rewritten as

$$\dot{V} = \tfrac{1}{2}e^T(A^TP + PA)e + (\tfrac{1}{2}u^TB^TPe + \tfrac{1}{2}e^TPBu) + (\tfrac{1}{2}\tilde{d}^TL^TPe + \tfrac{1}{2}e^TPL\tilde{d}) \tag{94}$$

Assumption: For given positive definite matrix Q and coefficients r and ρ there exists a positive definite matrix P, which is the solution of the following matrix equation

$$A^TP + PA = -Q + P(\tfrac{2}{r}BB^T - \tfrac{1}{\rho^2}LL^T)P \tag{95}$$

Moreover, the following feedback control law is applied to the system

$$u = -\tfrac{1}{r}B^TPe \tag{96}$$

By substituting Eq. (95) and Eq. (96) one obtains

$$\dot{V} = \tfrac{1}{2}e^T[-Q + P(\tfrac{2}{r}BB^T - \tfrac{1}{\rho^2}LL^T)P]e + e^TPB(-\tfrac{1}{r}B^TPe) + e^TPL\tilde{d} \Rightarrow \tag{97}$$

$$\begin{aligned}\dot{V} = -\tfrac{1}{2}e^TQe + \tfrac{1}{r}e^TPBB^TPe - \tfrac{1}{2\rho^2}e^TPLL^TPe \\ -\tfrac{1}{r}e^TPBB^TPe + e^TPL\tilde{d}\end{aligned} \tag{98}$$

which after intermediate operations gives

$$\dot{V} = -\frac{1}{2}e^T Q e - \frac{1}{2\rho^2}e^T PLL^T Pe + e^T PL\tilde{d} \tag{99}$$

or, equivalently

$$\dot{V} = -\frac{1}{2}e^T Q e - \frac{1}{2\rho^2}e^T PLL^T Pe + \frac{1}{2}e^T PL\tilde{d} + \frac{1}{2}\tilde{d}^T L^T Pe \tag{100}$$

Lemma: The following inequality holds

$$\frac{1}{2}e^T L\tilde{d} + \frac{1}{2}\tilde{d}L^T Pe - \frac{1}{2\rho^2}e^T PLL^T Pe \leq \frac{1}{2}\rho^2\tilde{d}^T\tilde{d} \tag{101}$$

Proof: The binomial $(\rho\alpha - \frac{1}{\rho}b)^2$ is considered. Expanding the left part of the above inequality one gets

$$\begin{array}{c}\rho^2a^2 + \frac{1}{\rho^2}b^2 - 2ab \geq 0 \Rightarrow \frac{1}{2}\rho^2a^2 + \frac{1}{2\rho^2}b^2 - ab \geq 0 \Rightarrow \\ ab - \frac{1}{2\rho^2}b^2 \leq \frac{1}{2}\rho^2a^2 \Rightarrow \frac{1}{2}ab + \frac{1}{2}ab - \frac{1}{2\rho^2}b^2 \leq \frac{1}{2}\rho^2a^2\end{array} \tag{102}$$

The following substitutions are carried out: $a = \tilde{d}$ and $b = e^T PL$ and the previous relation becomes

$$\frac{1}{2}\tilde{d}^T L^T Pe + \frac{1}{2}e^T PL\tilde{d} - \frac{1}{2\rho^2}e^T PLL^T Pe \leq \frac{1}{2}\rho^2\tilde{d}^T\tilde{d} \tag{103}$$

Eq. (103) is substituted in Eq. (100) and the inequality is enforced, thus giving

$$\dot{V} \leq -\frac{1}{2}e^T Q e + \frac{1}{2}\rho^2\tilde{d}^T\tilde{d} \tag{104}$$

Eq. (104) shows that the H_∞ tracking performance criterion is satisfied. The integration of $\dot{V}$ from 0 to T gives

$$\begin{array}{c}\int_0^T \dot{V}(t)dt \leq -\frac{1}{2}\int_0^T ||e||_Q^2 dt + \frac{1}{2}\rho^2\int_0^T ||\tilde{d}||^2 dt \Rightarrow \\ 2V(T) + \int_0^T ||e||_Q^2 dt \leq 2V(0) + \rho^2\int_0^T ||\tilde{d}||^2 dt\end{array} \tag{105}$$

Moreover, if there exists a positive constant $M_d > 0$ such that

$$\int_0^\infty ||\tilde{d}||^2 dt \leq M_d \tag{106}$$

then one gets

$$\int_0^\infty ||e||_Q^2 dt \leq 2V(0) + \rho^2 M_d \tag{107}$$

Thus, the integral $\int_0^\infty ||e||_Q^2 dt$ is bounded. Moreover, $V(T)$ is bounded and from the definition of the Lyapunov function V in Eq. (90) it becomes clear that $e(t)$ will be also bounded since $e(t) \in \Omega_e = \{e | e^T Pe \leq 2V(0) + \rho^2 M_d\}$. According to the above and with the use of Barbalat's Lemma one obtains $\lim_{t\to\infty} e(t) = 0$.

After following the stages of the stability proof one arrives at Eq. (104) which shows that the H-infinity tracking performance criterion holds. By selecting the attenuation coefficient ρ to be sufficiently small and in particular to satisfy $\rho^2 < ||e||_Q^2 / ||\tilde{d}||^2$ one has that the first derivative of the Lyapunov function is upper bounded by 0. This condition holds at each sampling instance and consequently global stability for the control loop can be concluded.

5.2 Robust state estimation with the use of the H_∞ Kalman Filter

The control loop has to be implemented with the use of information provided by a small number of sensors and by processing only a small number of state variables. To reconstruct the missing information about the state vector of the rotary double inverted pendulum it is proposed to use a filtering scheme and based on it to apply state estimation-based control [2-4]. By denoting as $A(k)$, $B(k)$, $C(k)$ the discrete-time equivalents of matrices A, B, C which constitute the linearized state-space model of Eq. (22), the recursion of the H_∞ Kalman Filter, for the model of the rotary double inverted pendulum, can be formulated in terms of a *measurement update* and a *time update* part

Measurement update:

$$\begin{array}{l} D(k) = [I - \theta W(k)P^-(k) + C^T(k)R(k)^{-1}C(k)P^-(k)]^{-1} \\ K(k) = P^-(k)D(k)C^T(k)R(k)^{-1} \\ \hat{x}(k) = \hat{x}^-(k) + K(k)[y(k) - C\hat{x}^-(k)] \end{array} \tag{108}$$

Time update:

$$\begin{array}{l} \hat{x}^-(k+1) = A(k)x(k) + B(k)u(k) \\ P^-(k+1) = A(k)P^-(k)D(k)A^T(k) + Q(k) \end{array} \tag{109}$$

where it is assumed that parameter θ is sufficiently small to assure that the covariance matrix $P^-(k)^{-1} - \theta W(k) + C^T(k)R(k)^{-1}C(k)$ will be positive definite. When $\theta = 0$ the H_∞ Kalman Filter becomes equivalent to the standard Kalman Filter. One can measure only a part of the state vector of the rotary double inverted pendulum, for instance state variables x_1, x_3 and x_5 (turn angles of the joints) and can estimate through filtering the rest of the state vector elements (x_2, x_4, and x_6 (angular velocities. Moreover, the proposed Kalman filtering method can be used for sensor fusion purposes.

6 Generalization of results for the parallel double inverted pendulum

6.1 Dynamic model of the double parallel pendulum

It will be shown that the proposed nonlinear optimal control method is not only suitable for the stabilization of the rotary double inverted pendulum but can be also used in more underactuated nonlinear dynamical systems. To this end, the parallel double inverted pendulum is used as a case study[45- 47]. The diagram of the parallel double inverted pendulum is given in Fig. 3

The parameters of the dynamic model of the parallel double inverted pendulum are: (i) θ_{p_1} is the turn angle of the first pendulum, l_{p_1} is the length of the first pendulum, m_{p_1} and I_{p_1} are the mass and the moment of inertia of the first pendulum respectively, c_1 is the first pendulum's friction coefficient, (ii) θ_{p_2} is the turn angle of the second pendulum, l_{p_2} is the length of the second pendulum, m_{p_2} and I_{p_2} are the mass and the moment of inertia of the second pendulum respectively, c_2 is the second pendulum's friction coefficient. Finally, g is the acceleration of gravity. The dynamic model of the parallel double inverted pendulum is given by

$$\begin{array}{l} I_{p_1}\ddot{\theta}_{p_1} + m_{p_1}l_{p_1}\ddot{x}cos(\theta_{p_1}) - m_{p_1}gl_{p_1}sin(\theta_{p_1}) + c_1\dot{\theta}_{p_1} = 0 \\ I_{p_2}\ddot{\theta}_{p_2} + m_{p_2}l_{p_2}\ddot{x}cos(\theta_{p_2}) - m_{p_2}gl_{p_2}sin(\theta_{p_2}) + c_2\dot{\theta}_{p_2} = 0 \end{array} \tag{110}$$

The control input of this dynamical system is taken to be the cart's acceleration $\ddot{x} = u$, thus one has

$$\begin{array}{l} I_{p_1}\ddot{\theta}_{p_1} + m_{p_1}l_{p_1}u{\cdot}cos(\theta_{p_1}) - m_{p_1}gl_{p_1}sin(\theta_{p_1}) + c_1\dot{\theta}_{p_1} = 0 \\ I_{p_2}\ddot{\theta}_{p_2} + m_{p_2}l_{p_2}u{\cdot}cos(\theta_{p_2}) - m_{p_2}gl_{p_2}sin(\theta_{p_2}) + c_2\dot{\theta}_{p_2} = 0 \end{array} \tag{111}$$

or equivalently

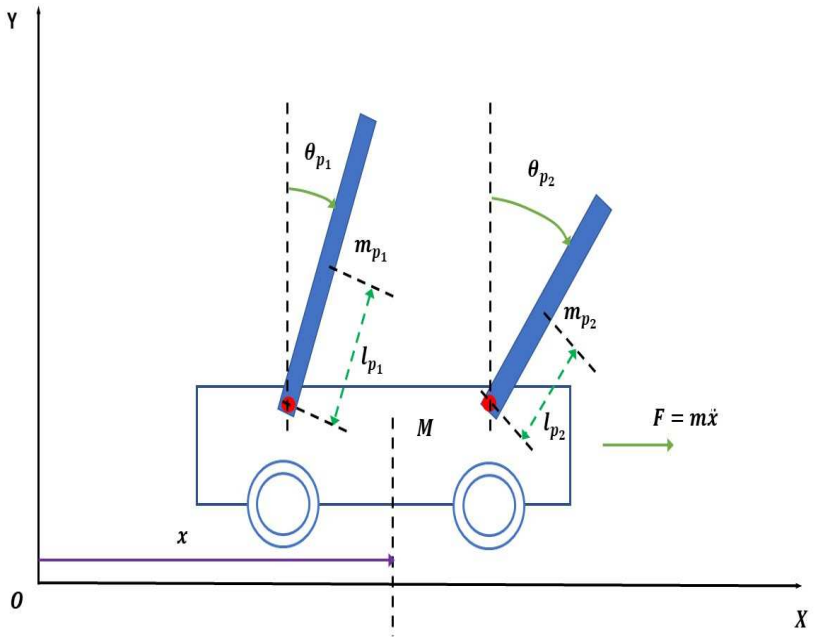

Figure 3: Diagram of the parallel double inverted pendulum - System 1

$$\begin{aligned}\ddot{\theta}_{p_1} &= \tfrac{m_{p_1}}{I_{p_1}} g l_{p_1} sin(\theta_{p_1}) - \tfrac{c_1}{I_{p_1}}\dot{\theta}_{p_1} - \tfrac{m_{p_1}}{I_{p_1}} l_{p_1} \cdot cos(\theta_{p_1}) u \\ \ddot{\theta}_{p_2} &= \tfrac{m_{p_2}}{I_{p_2}} g l_{p_2} sin(\theta_{p_2}) - \tfrac{c_2}{I_{p_2}}\dot{\theta}_{p_2} - \tfrac{m_{p_2}}{I_{p_2}} l_{p_2} \cdot cos(\theta_{p_2}) u\end{aligned} \tag{112}$$

The following state vector is defined $x = [x_1, x_2, x_3, x_4]^T = [\theta_{p_1}, \dot{\theta}_{p_1}, \theta_{p_2}, \dot{\theta}_{p_2}]^T$. Thus, the dynamic model of the parallel double inverted pendulum becomes:

$$\begin{aligned}\dot{x}_1 &= x_2 \\ \dot{x}_2 &= \tfrac{m_{p_1}}{I_{p_1}} g l_{p_1} sin(x_1) - \tfrac{c_1}{I_{p_1}} x_2 - \tfrac{m_{p_1}}{I_{p_1}} l_{p_1} \cdot cos(x_1) u \\ \dot{x}_3 &= x_4 \\ \dot{x}_4 &= \tfrac{m_{p_2}}{I_{p_2}} g l_{p_2} sin(x_3) - \tfrac{c_2}{I_{p_2}} x_4 - \tfrac{m_{p_2}}{I_{p_2}} l_{p_2} \cdot cos(x_3) u\end{aligned} \tag{113}$$

In matrix form, the state-space model of the parallel double inverted pendulum becomes

$$\begin{pmatrix}\dot{x}_1 \\ \dot{x}_2 \\ \dot{x}_3 \\ \dot{x}_4\end{pmatrix} = \begin{pmatrix} x_2 \\ \tfrac{m_{p_1}}{I_{p_1}} g l_{p_1} sin(x_1) - \tfrac{c_1}{I_{p_1}} x_2 \\ x_4 \\ \tfrac{m_{p_2}}{I_{p_2}} g l_{p_2} sin(x_3) - \tfrac{c_2}{I_{p_2}} x_4 \end{pmatrix} + \begin{pmatrix} 0 \\ -\tfrac{m_{p_1}}{I_{p_1}} l_{p_1} \cdot cos(x_1) \\ 0 \\ -\tfrac{m_{p_2}}{I_{p_2}} l_{p_2} \cdot cos(x_3) \end{pmatrix} u \tag{114}$$

and finally, the dynamic model of the parallel double inverted pendulum can be written in the nonlinear affine-in-the-input state-space form

$$\dot{x} = f(x) + g(x)u \tag{115}$$

where $x \in R^{4\times1}$, $f(x) \in R^{4\times1}$, $g(x) \in R^{4\times1}$ and $u \in R$, The system is underactuated, and is differentially flat for small turn angles of the poles, having the flat output $y = x_1 - x_3$.

6.2 Approximate linearization of the parallel double inverted pendulum

The state-space model of the parallel double inverted pendulum undergoes approximate linearization around the temporary operating point (x^*, u^*), where x^* is the present value of the system's state vector and u^* is the last sampled value of the control inputs vector. The linearization takes place at each sampling instance through the computation of the system's Jacobian matrices. The modelling error which is due to the truncation of higher-order terms in the Taylor series, is considered to be a perturbation which is asymptotically compensated by the robustness of the control algorithm. The linearization process allows for substituting the initial nonlinear state-space model

$$\dot{x} = f(x) + g(x)u \tag{116}$$

with the approximately linearized model

$$\dot{x} = Ax + Bu + \tilde{d} \tag{117}$$

where A, B are the Jacobian matrices of the system which are given by

$$\begin{array}{c} A = \nabla_x[f(x) + g(x)u] \mid_{(x^*,u^*)} \Rightarrow \\ A = \nabla_x[f(x)] \mid_{(x^*,u^*)} + [\nabla_x g(x)]u \mid_{(x^*,u^*)} \end{array} \tag{118}$$

$$\begin{array}{c} B = \nabla_u[f(x) + g(x)u] \mid_{(x^*,u^*)} \Rightarrow \\ B = g(x) \mid_{(x^*,u^*)} \end{array} \tag{119}$$

while $\tilde{d}$ is the cumulative disturbance vector that may comprise (i) exogenous perturbations, (ii) modelling errors due to higher-order terms in the Taylor series, (iii) sensor measurement noise of any distribution.

In this linearization process matrix $A = \nabla_x[f(x) + g(x)u] \mid_{(x^*,u^*)}$ is computed as follows:

$$A = \begin{pmatrix} 0 & 1 & 0 & 0 \\ \frac{m_{p_1}}{I_{p_1}} g l_{p_1} cos(x_1) + \frac{m_{p_1}}{I_{p_1}} l_{p_1} sin(x_1)u & -\frac{c_1}{I_{p_1}} & 0 & 0 \\ 0 & 0 & 0 & 1 \\ 0 & 0 & \frac{m_{p_2}}{I_{p_2}} g l_{p_2} cos(x_3) + \frac{m_{p_3}}{I_{p_3}} l_{p_3} sin(x_3)u & -\frac{c_2}{I_{p_2}} \end{pmatrix} \mid_{(x^*,u^*)} \tag{120}$$

while matrix $B = \nabla_u[f(x) + g(x)u] \mid_{(x^*,u^*)}$ is given by:

$$B = \begin{pmatrix} 0 \\ -\frac{m_{p_1}}{I_{p_1}} l_{p_1} \cdot cos(x_1) \\ 0 \\ -\frac{m_{p_2}}{I_{p_2}} l_{p_2} \cdot cos(x_3) \end{pmatrix} \mid_{(x^*,u^*)} \tag{121}$$

7 Simulation tests

7.1 Control of the rotary double inverted pendulum

The global stability properties of the control method and the elimination of the state vector's tracking error which were previously proven through Lyapunov analysis are further confirmed through simulation experiments. To implement the nonlinear optimal control scheme the algebraic Riccati equation of Eq. (95) had to be solved at each time-step of the control method. The solution of the Riccati equation was obtained with the use of Matlab's *aresolv()* function. Indicative values for the parameters of the model

of the rotary double inverted pendulum have been given in [5]. In the presented simulation tests the parameters of the rotary double inverted pendulum have been: (i) lengths of links $l_0 = 1.5m$, $l_1 = 0.60m$, $l_2 = 0.65m$, (ii) moments of inertia of the links $J_0 = 1.230kg{\cdot}m^2$, $J_1 = 0.720kg{\cdot}m^2$, $J_2 = 0.590kg{\cdot}m^2$, (iii) distances from the joint to the center of gravity of the links $r_1 = 0.065m$, $r_2 = 0.040$m, (iv) masses of the links $m_1 = 1.60kg$, $m_2 = 1.50kg$, (v) viscous friction coefficients $\bar{C}_0 = 6.000$, $\bar{C}_1 = 0.0058$, $\bar{C}_2 = 0.060$. The acceleration of gravity was $g = 9.8m/sec^2$. The obtained results are depicted in Fig. 4 to Fig. 11. In these diagrams the real values of the state variables of the rotary double inverted pendulum are shown in blue colour, the estimated values which have been obtained with the use of the H-infinity Kalman Filter are depicted in green while the associated setpoints are plotted in red.

The simulation experiments have confirmed that the proposed nonlinear optimal control method for the rotary double inverted pendulum achieves fast and accurate tracking of reference setpoints under moderate variations of the control inputs. The transient performance of the control method depends on the selection of the parameters of the above-noted Riccati equation r, ρ and Q. For relatively small values of r the state vectors' tracking error is eliminated. For relatively large values of the diagonal elements of gain matrix Q the speed of convergence of the state variables to the associated setpoints is raised. Moreover, the smallest value of the attenuation coefficient ρ for which a valid solution is obtained from the Riccati equation in the form of a positive definite and symmetric matrix P is the one that achieves maximum robustness for the control loop.

To elaborate on the tracking performance and on the robustness of the proposed nonlinear optimal control method for the rotary double inverted pendulum the following Tables are given: (i) Table Ia which provides information about the accuracy of tracking of the reference setpoints by the state variables of the rotary double inverted pendulum's state-space model, (iia) Table IIa which provides information about the robustness of the control method to parametric changes in the model of the rotary double inverted pendulum's dynamics (change $\Delta a\%$ in the moment of inertia J_0 of the first link), (iii) Table IIIa which provides information about the precision in state variables' estimation that is achieved by the H-infinity Kalman Filter, (iv) Table IVa which provides the approximate convergence times of the rotary double inverted pendulum's state variables to the associated setpoints.

Table Ia: rotary double inverted pendulum

Tracking RMSE for the rotary pendulum in the disturbance-free case $\times 10^{-3}$

	$RMSE_{x_1}$	$RMSE_{x_2}$	$RMSE_{x_3}$	$RMSE_{x_4}$	$RMSE_{x_5}$	$RMSE_{x_6}$
test_1	0.0233	0.0185	0.0001	0.0009	0.0012	0.0007
test_2	0.0592	0.0241	0.0008	0.0014	0.0658	0.0223
test_3	0.1010	0.0422	0.0014	0.0013	0.1145	0.0402
test_4	0.0986	0.0424	0.0014	0.0014	0.1144	0.0400
test_5	0.1009	0.0423	0.0014	0.0014	0.1143	0.0400
test_6	0.0759	0.0517	0.0011	0.0013	0.0982	0.0320
test_7	0.0410	0.0336	0.0006	0.0011	0.0470	0.0161
test_8	0.0925	0.0377	0.0012	0.0013	0.1028	0.0359

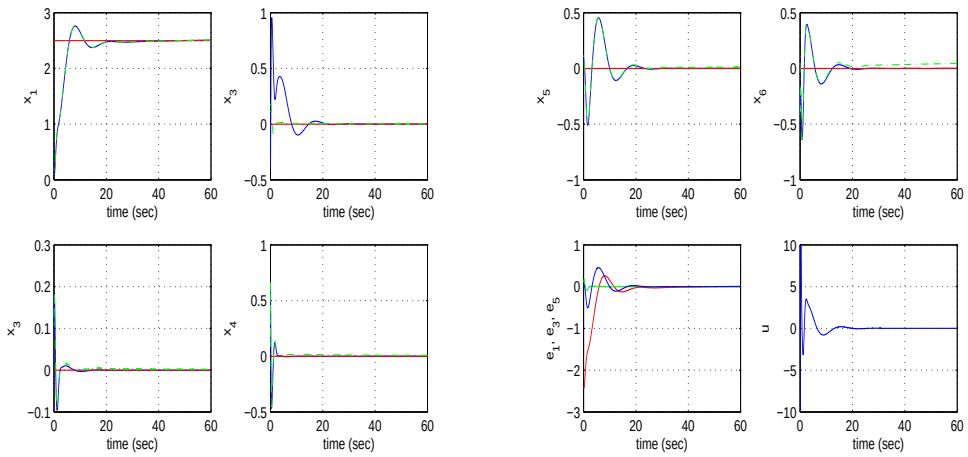

(a) **(b)**

Figure 4: Tracking of setpoint 1 for the rotary double inverted pendulum (double Furuta pendulum): (a) convergence of state variable $x_1 = \theta_0$, $x_2 = \dot{\theta}_0$, $x_3 = \theta_1$, $x_4 = \dot{\theta}_1$ to their reference setpoints (red line: setpoint, blue line: real value, green line: estimated value), and variations of the control u (torque τ) at the first joint) (b) convergence of state variable $x_5 = \theta_2$, $x_6 = \dot{\theta}_2$ to their reference setpoints (red line: setpoint, blue line: real value, green line: estimated value), variation of tracking errors e_1 (red), e_3 (green), e_5 (blue) and variations of the control u (torque τ) at the first joint)

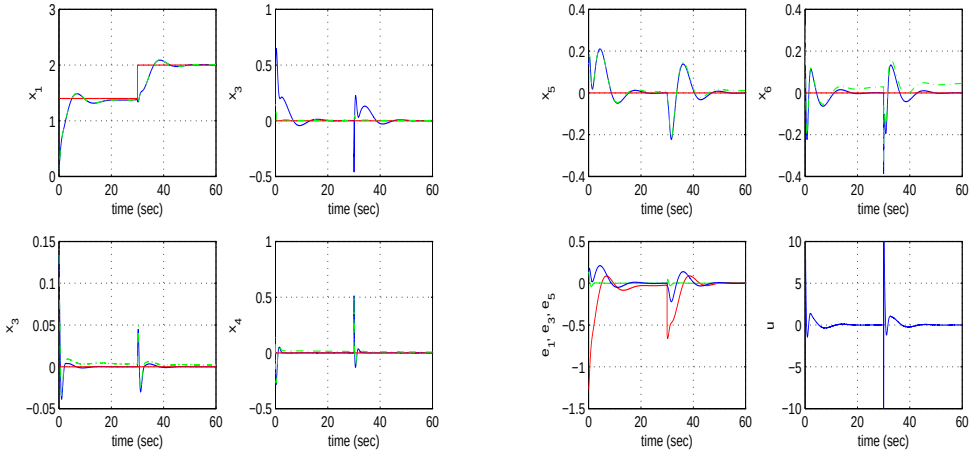

(a) **(b)**

Figure 5: Tracking of setpoint 2 for the rotary double inverted pendulum (double Furuta pendulum): (a) convergence of state variable $x_1 = \theta_0$, $x_2 = \dot{\theta}_0$, $x_3 = \theta_1$, $x_4 = \dot{\theta}_1$ to their reference setpoints (red line: setpoint, blue line: real value, green line: estimated value), and variations of the control u (torque τ) at the first joint) (b) convergence of state variable $x_5 = \theta_2$, $x_6 = \dot{\theta}_2$ to their reference setpoints (red line: setpoint, blue line: real value, green line: estimated value), variation of tracking errors e_1 (red), e_3 (green), e_5 (blue) and variations of the control u (torque τ) at the first joint)

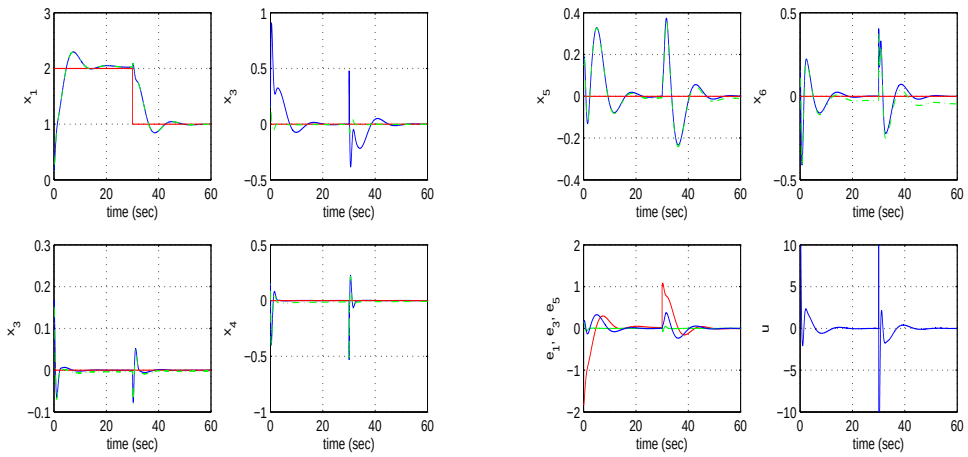

(a) **(b)**

Figure 6: Tracking of setpoint 3 for the rotary double inverted pendulum (double Furuta pendulum): (a) convergence of state variable $x_1 = \theta_0$, $x_2 = \dot{\theta}_0$, $x_3 = \theta_1$, $x_4 = \dot{\theta}_1$ to their reference setpoints (red line: setpoint, blue line: real value, green line: estimated value), and variations of the control u (torque τ) at the first joint) (b) convergence of state variable $x_5 = \theta_2$, $x_6 = \dot{\theta}_2$ to their reference setpoints (red line: setpoint, blue line: real value, green line: estimated value), variation of tracking errors e_1 (red), e_3 (green), e_5 (blue) and variations of the control u (torque τ) at the first joint)

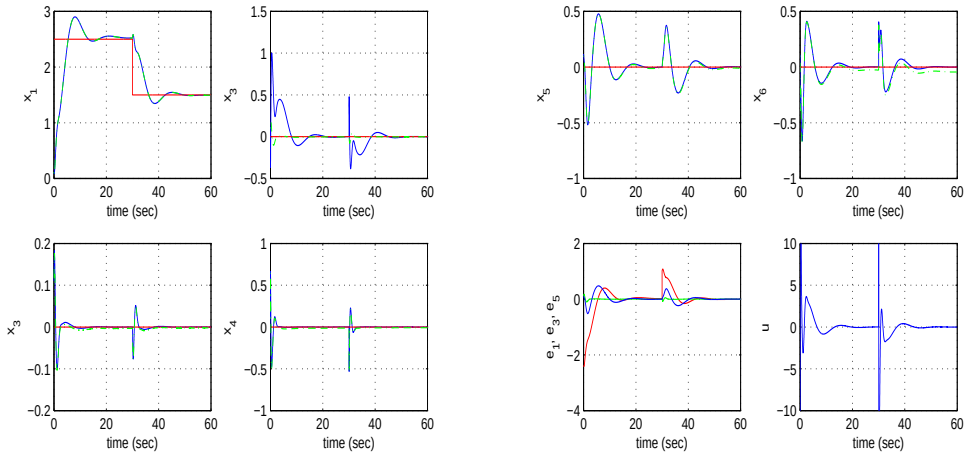

(a) **(b)**

Figure 7: Tracking of setpoint 4 for the rotary double inverted pendulum (double Furuta pendulum): (a) convergence of state variable $x_1 = \theta_0$, $x_2 = \dot{\theta}_0$, $x_3 = \theta_1$, $x_4 = \dot{\theta}_1$ to their reference setpoints (red line: setpoint, blue line: real value, green line: estimated value), and variations of the control u (torque τ) at the first joint) (b) convergence of state variable $x_5 = \theta_2$, $x_6 = \dot{\theta}_2$ to their reference setpoints (red line: setpoint, blue line: real value, green line: estimated value), variation of tracking errors e_1 (red), e_3 (green), e_5 (blue) and variations of the control u (torque τ) at the first joint)

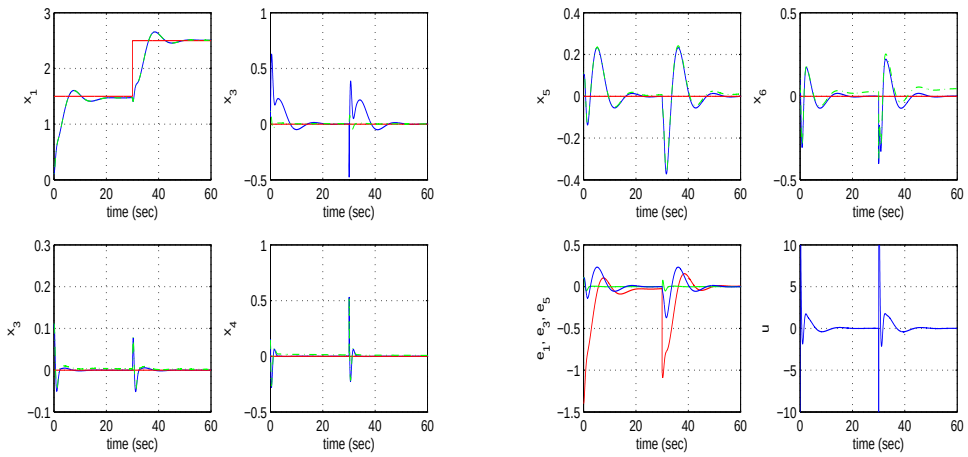

(a) **(b)**

Figure 8: Tracking of setpoint 5 for the rotary double inverted pendulum (double Furuta pendulum): (a) convergence of state variable $x_1 = \theta_0$, $x_2 = \dot{\theta}_0$, $x_3 = \theta_1$, $x_4 = \dot{\theta}_1$ to their reference setpoints (red line: setpoint, blue line: real value, green line: estimated value), and variations of the control u (torque τ) at the first joint) (b) convergence of state variable $x_5 = \theta_2$, $x_6 = \dot{\theta}_2$ to their reference setpoints (red line: setpoint, blue line: real value, green line: estimated value), variation of tracking errors e_1 (red), e_3 (green), e_5 (blue) and variations of the control u (torque τ) at the first joint)

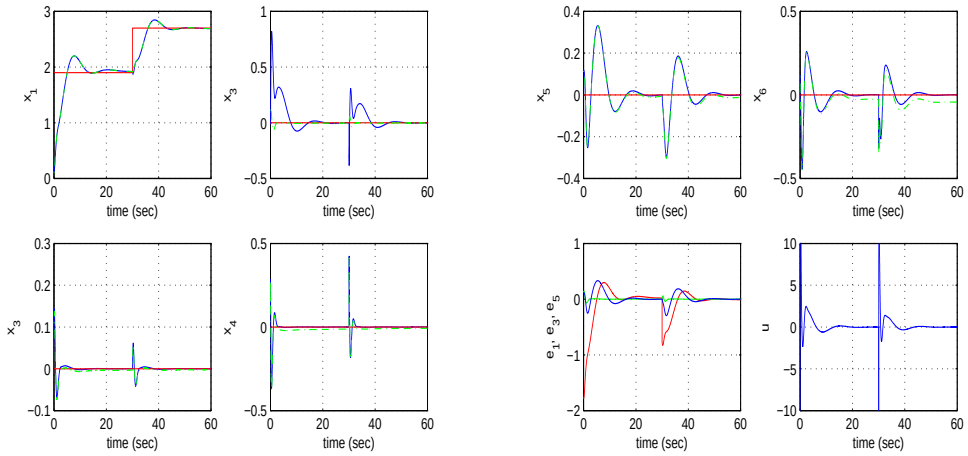

(a) **(b)**

Figure 9: Tracking of setpoint 6 for the rotary double inverted pendulum (double Furuta pendulum): (a) convergence of state variable $x_1 = \theta_0$, $x_2 = \dot{\theta}_0$, $x_3 = \theta_1$, $x_4 = \dot{\theta}_1$ to their reference setpoints (red line: setpoint, blue line: real value, green line: estimated value), and variations of the control u (torque τ) at the first joint) (b) convergence of state variable $x_5 = \theta_2$, $x_6 = \dot{\theta}_2$ to their reference setpoints (red line: setpoint, blue line: real value, green line: estimated value), variation of tracking errors e_1 (red), e_3 (green), e_5 (blue) and variations of the control u (torque τ) at the first joint)

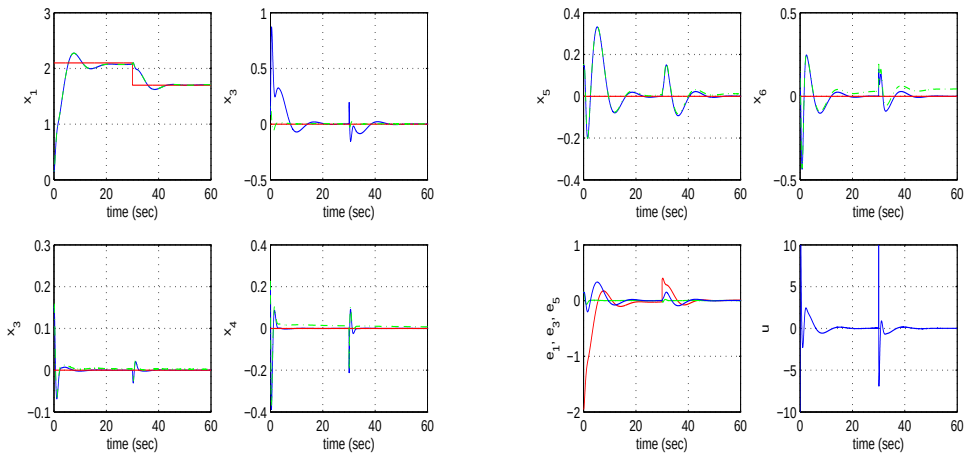

(a) **(b)**

Figure 10: Tracking of setpoint 7 for the rotary double inverted pendulum (double Furuta pendulum): (a) convergence of state variable $x_1 = \theta_0$, $x_2 = \dot{\theta}_0$, $x_3 = \theta_1$, $x_4 = \dot{\theta}_1$ to their reference setpoints (red line: setpoint, blue line: real value, green line: estimated value), and variations of the control u (torque τ) at the first joint) (b) convergence of state variable $x_5 = \theta_2$, $x_6 = \dot{\theta}_2$ to their reference setpoints (red line: setpoint, blue line: real value, green line: estimated value), variation of tracking errors e_1 (red), e_3 (green), e_5 (blue) and variations of the control u (torque τ) at the first joint)

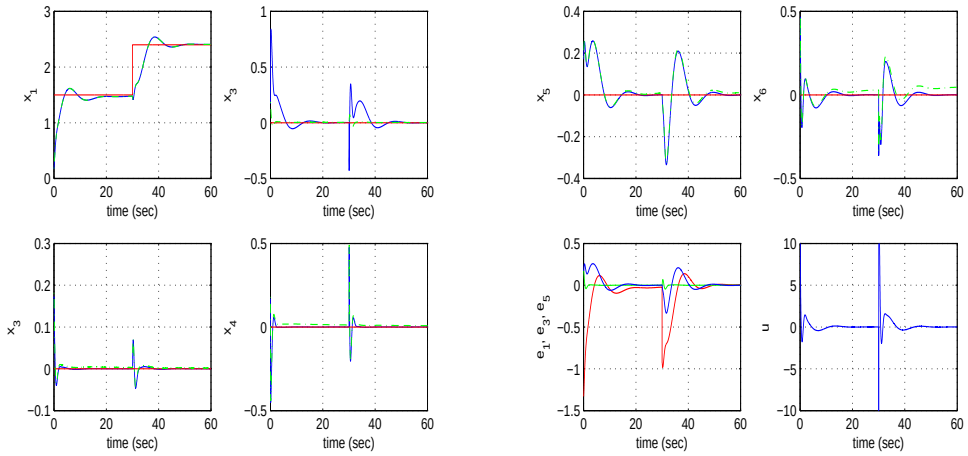

(a) **(b)**

Figure 11: Tracking of setpoint 8 for the rotary double inverted pendulum (double Furuta pendulum): (a) convergence of state variable $x_1 = \theta_0$, $x_2 = \dot{\theta}_0$, $x_3 = \theta_1$, $x_4 = \dot{\theta}_1$ to their reference setpoints (red line: setpoint, blue line: real value, green line: estimated value), and variations of the control u (torque τ) at the first joint) (b) convergence of state variable $x_5 = \theta_2$, $x_6 = \dot{\theta}_2$ to their reference setpoints (red line: setpoint, blue line: real value, green line: estimated value), variation of tracking errors e_1 (red), e_3 (green), e_5 (blue) and variations of the control u (torque τ) at the first joint)

Table IIa: rotary double inverted pendulum						
Tracking RMSE for the rotary pendulum in the case of disturbances $\times 10^{-3}$						
$\Delta a\%$	$RMSE_{x_1}$	$RMSE_{x_2}$	$RMSE_{x_3}$	$RMSE_{x_4}$	$RMSE_{x_5}$	$RMSE_{x_6}$
0%	0.0592	0.0241	0.0008	0.0014	0.0658	0.0223
10%	0.0525	0.0249	0.0008	0.0013	0.0674	0.0239
20%	0.0459	0.0256	0.0009	0.0013	0.0691	0.0258
30%	0.0400	0.0265	0.0009	0.0012	0.0741	0.0277
40%	0.0353	0.0276	0.0009	0.0013	0.0722	0.0296
50%	0.0313	0.0287	0.0008	0.0014	0.0735	0.0352
60%	0.0287	0.0301	0.0009	0.0012	0.0747	0.0337

Table IIIa: rotary double inverted pendulum						
RMSE for the estimation performed by the H-infinity KF $\times 10^{-3}$						
	$RMSE_{x_1}$	$RMSE_{x_2}$	$RMSE_{x_3}$	$RMSE_{x_4}$	$RMSE_{x_5}$	$RMSE_{x_6}$
test_1	0.0200	0.0004	0.0208	0.2192	0.0438	0.9570
test_2	0.0189	0.0004	0.0201	0.2194	0.0412	0.9562
test_3	0.0191	0.0004	0.0172	0.2193	0.0389	0.9561
test_4	0.0203	0.0004	0.0231	0.2190	0.0443	0.9576
test_5	0.0214	0.0005	0.0206	0.2193	0.0389	0.9564
test_6	0.0189	0.0004	0.0215	0.2193	0.0389	0.9564
test_7	0.0189	0.0004	0.0234	0.2195	0.0409	0.9557
test_8	0.0189	0.0004	0.0229	0.2195	0.0394	0.9557

Table IVa: rotary double inverted pendulum						
Convergence time (sec) for state variables x_1 **to** x_6						
	$T_s\ x_1$	$T_s\ x_2$	$T_s\ x_3$	$T_s\ x_4$	$T_s\ x_5$	$T_s\ x_6$
test_1	18.0	20.0	8.0	4.0	23.0	19.0
test_2	15.0	13.0	8.0	3.0	21.0	18.0
test_3	12.0	15.0	7.0	4.0	21.0	18.0
test_4	16.0	15.0	9.0	4.0	21.0	19.0
test_5	18.0	13.0	4.0	4.0	20.0	18.0
test_6	12.0	15.0	6.0	4.0	21.0	18.0
test_7	10.0	14.0	8.0	4.0	21.0	18.0
test_8	16.0	13.0	4.0	4.0	20.0	11.0

7.2 Control of the parallel double inverted pendulum

Simulation experiments about the performance of the nonlinear optimal control method in the case of the parallel double inverted pendulum are given in Fig. 12 to Fig. 19. The parameters of the dynamic model of the parallel double inverted pendulum were: $m_{p_1} = 0.80kg$, $l_{p_1} = 0.70m$, $I_{p_1} = 0.40kgm^2$, $c_1 = 0.12$, $m_{p_2} = 0.85kg$, $l_{p_2} = 0.85m$, , $I_{p_2} = 0.54kgm^2$, $c_2 = 0.15$ and $g = 10m/sec^2$. Through the obtained results it can be confirmed that the nonlinear optimal control method achieves fast stabilization of the parallel double inverted pendulum under moderate variations of the control inputs.

To elaborate on the tracking performance and on the robustness of the proposed nonlinear optimal control method for the parallel double inverted pendulum the following Tables are given: (i) Table Ib which provides information about the accuracy of tracking of the reference setpoints by the state variables of the parallel double inverted pendulum's state-space model, (ii) Table IIb which provides information about the robustness of the control method to parametric changes in the model of the parallel double inverted pendulum's dynamics (change $\Delta a\%$ in the friction coefficients c_1, c_2 of the parallel double inverted pendulum), (iii) Table IIIb which provides information about the precision in state variables' estimation that

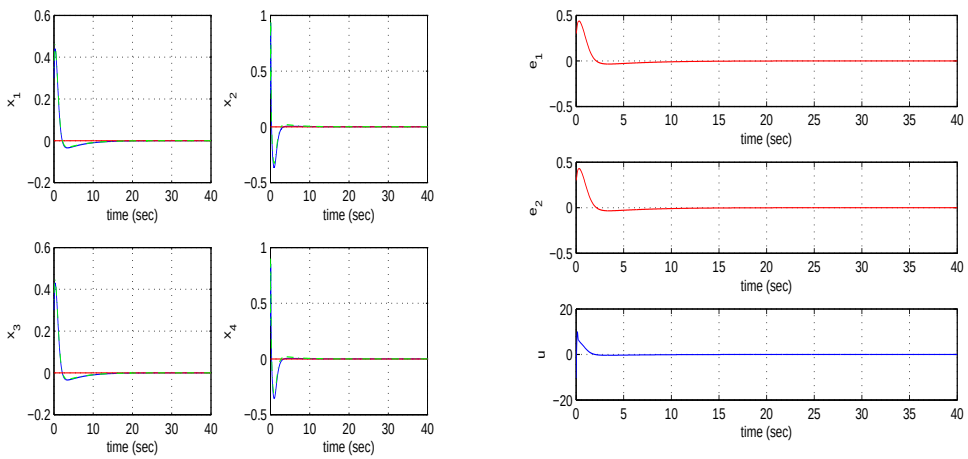

(a) **(b)**

Figure 12: Tracking of setpoint 1 for the parallel double inverted pendulum (cart with double inverted pendulum): (a) convergence of state variable $x_1 = \theta_{p_1}$, $x_2 = \dot{\theta}_{p_1}$, $x_3 = \theta_2$, $x_4 = \dot{\theta}_{p_2}$ to their reference setpoints (red line: setpoint, blue line: real value, green line: estimated value), (b) variation of tracking errors e_1, e_3, and variations of the control input u (acceleration of the cart)

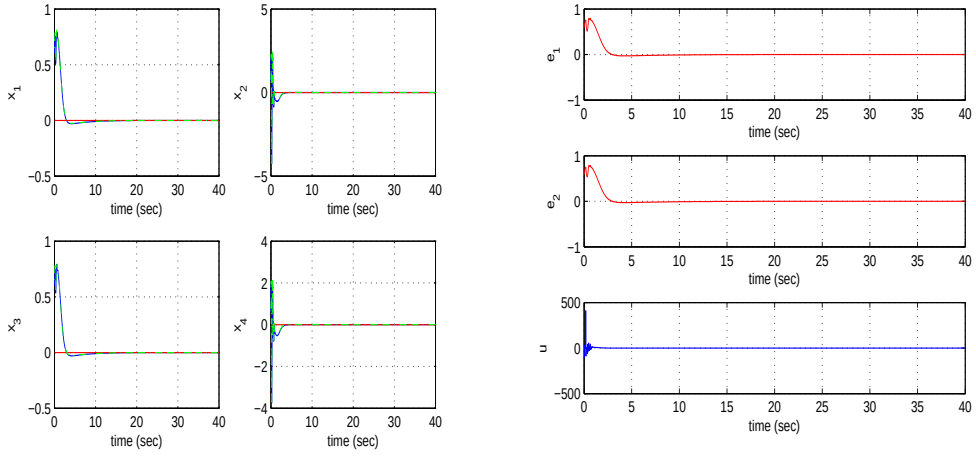

(a) **(b)**

Figure 13: Tracking of setpoint 2 for the parallel double inverted pendulum (cart with double inverted pendulum): (a) convergence of state variable $x_1 = \theta_{p_1}$, $x_2 = \dot{\theta}_{p_1}$, $x_3 = \theta_2$, $x_4 = \dot{\theta}_{p_2}$ to their reference setpoints (red line: setpoint, blue line: real value, green line: estimated value), (b) variation of tracking errors e_1, e_3, and variations of the control input u (acceleration of the cart)

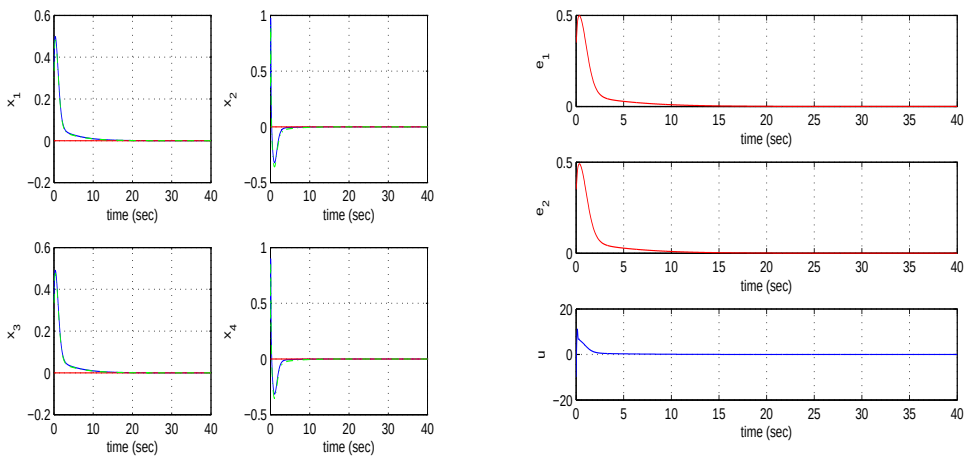

(a) **(b)**

Figure 14: Tracking of setpoint 3 for the parallel double inverted pendulum (cart with double inverted pendulum): (a) convergence of state variable $x_1 = \theta_{p_1}$, $x_2 = \dot{\theta}_{p_1}$, $x_3 = \theta_2$, $x_4 = \dot{\theta}_{p_2}$ to their reference setpoints (red line: setpoint, blue line: real value, green line: estimated value), (b) variation of tracking errors e_1, e_3, and variations of the control input u (acceleration of the cart)

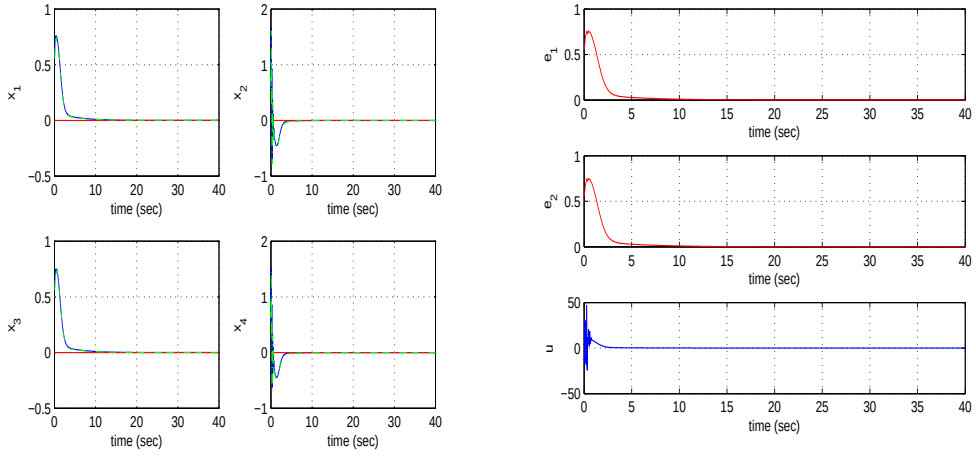

(a) **(b)**

Figure 15: Tracking of setpoint 4 for the parallel double inverted pendulum (cart with double inverted pendulum): (a) convergence of state variable $x_1 = \theta_{p_1}$, $x_2 = \dot{\theta}_{p_1}$, $x_3 = \theta_2$, $x_4 = \dot{\theta}_{p_2}$ to their reference setpoints (red line: setpoint, blue line: real value, green line: estimated value), (b) variation of tracking errors e_1, e_3, and variations of the control input u (acceleration of the cart)

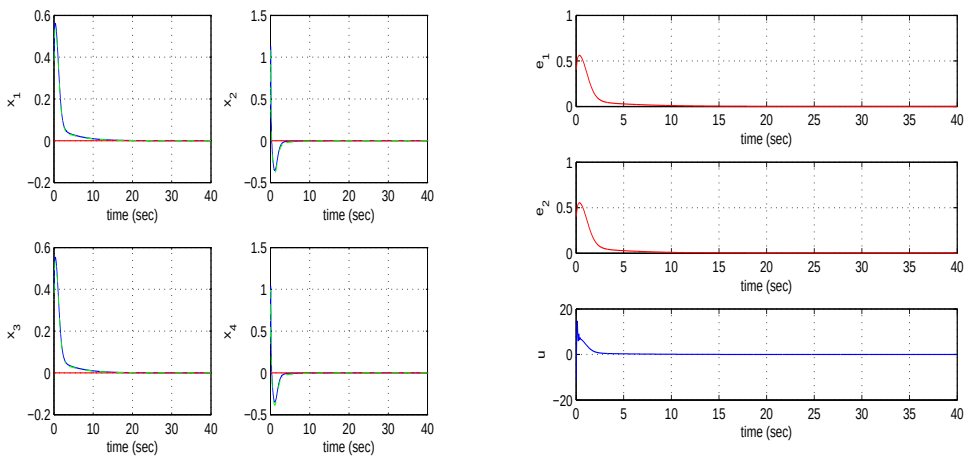

(a) **(b)**

Figure 16: Tracking of setpoint 5 for the parallel double inverted pendulum (cart with double inverted pendulum): (a) convergence of state variable $x_1 = \theta_{p_1}$, $x_2 = \dot{\theta}_{p_1}$, $x_3 = \theta_2$, $x_4 = \dot{\theta}_{p_2}$ to their reference setpoints (red line: setpoint, blue line: real value, green line: estimated value), (b) variation of tracking errors e_1, e_3, and variations of the control input u (acceleration of the cart)

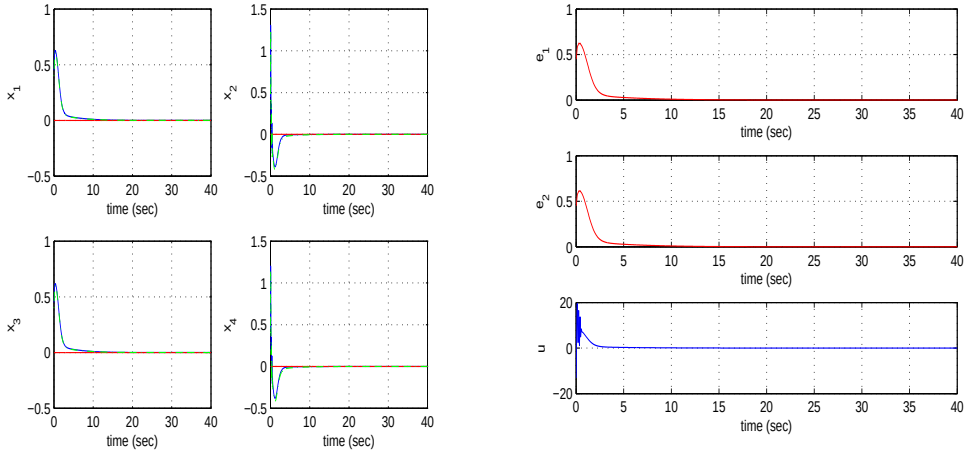

(a) **(b)**

Figure 17: Tracking of setpoint 6 for the parallel double inverted pendulum (cart with double inverted pendulum): (a) convergence of state variable $x_1 = \theta_{p_1}$, $x_2 = \dot{\theta}_{p_1}$, $x_3 = \theta_2$, $x_4 = \dot{\theta}_{p_2}$ to their reference setpoints (red line: setpoint, blue line: real value, green line: estimated value), (b) variation of tracking errors e_1, e_3, and variations of the control input u (acceleration of the cart)

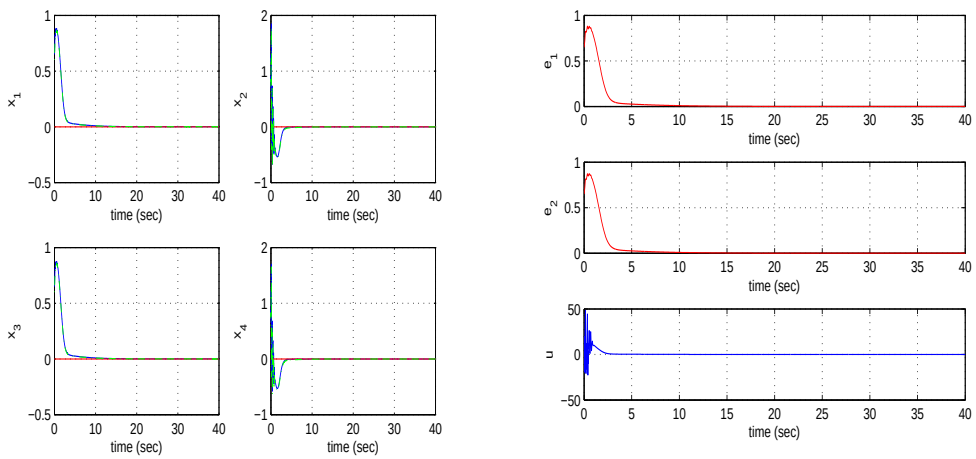

(a) **(b)**

Figure 18: Tracking of setpoint 7 for the parallel double inverted pendulum (cart with double inverted pendulum): (a) convergence of state variable $x_1 = \theta_{p_1}$, $x_2 = \dot{\theta}_{p_1}$, $x_3 = \theta_2$, $x_4 = \dot{\theta}_{p_2}$ to their reference setpoints (red line: setpoint, blue line: real value, green line: estimated value), (b) variation of tracking errors e_1, e_3, and variations of the control input u (acceleration of the cart)

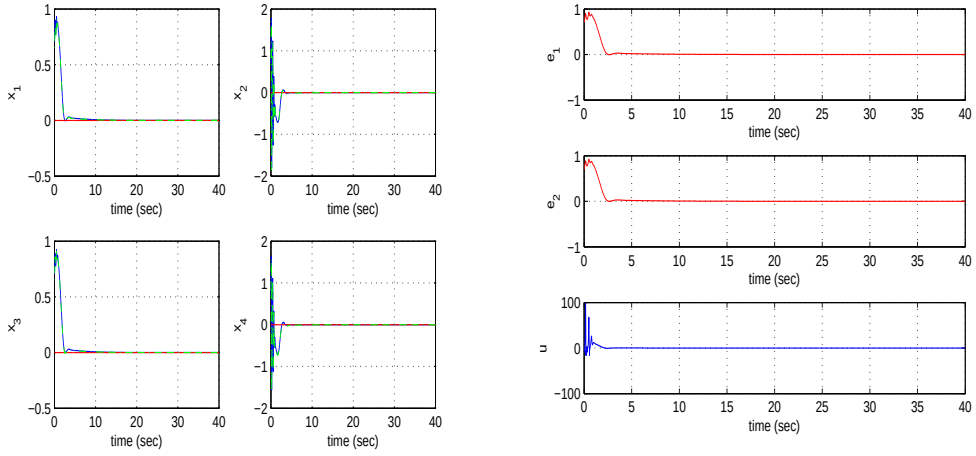

(a) **(b)**

Figure 19: Tracking of setpoint 8 for the parallel double inverted pendulum (cart with double inverted pendulum): (a) convergence of state variable $x_1 = \theta_{p_1}$, $x_2 = \dot{\theta}_{p_1}$, $x_3 = \theta_2$, $x_4 = \dot{\theta}_{p_2}$ to their reference setpoints (red line: setpoint, blue line: real value, green line: estimated value), (b) variation of tracking errors e_1, e_3, and variations of the control input u (acceleration of the cart)

is achieved by the H-infinity Kalman Filter, (iv) Table IVb which provides the approximate convergence times of the parallel double inverted pendulum's state variables to the associated setpoints.

Table Ib: parallel double inverted pendulum

Tracking RMSE for the parallel pendulum in the disturbance-free case$\times 10^{-6}$

	$RMSE_{x_1}$	$RMSE_{x_2}$	$RMSE_{x_3}$	$RMSE_{x_4}$
test_1	0.4317	0.1166	0.4318	0.1166
test_2	0.4220	0.1162	0.4321	0.1162
test_3	0.4314	0.1163	0.4315	0.1165
test_4	0.4325	0.1163	0.4326	0.1163
test_5	0.4315	0.1169	0.4316	0.1169
test_6	0.4325	0.1167	0.4326	0.1167
test_7	0.3985	0.1069	0.3985	0.1070
test_8	0.2981	0.0777	0.2882	0.0777

Table IIb: parallel double inverted pendulum

Tracking RMSE for the parallel pendulum in the case of disturbances$\times 10^{-5}$

$\Delta a\%$	$RMSE_{x_1}$	$RMSE_{x_2}$	$RMSE_{x_3}$	$RMSE_{x_4}$
0%	0.0431	0.0116	0.0431	0.0116
10%	0.0840	0.0208	0.0840	0.0208
20%	0.1403	0.0326	0.1403	0.0326
30%	0.2138	0.0472	0.2138	0.0472
40%	0.3064	0.0647	0.3063	0.0647
50%	0.4197	0.0352	0.4169	0.0852
60%	0.5564	0.1098	0.5583	0.1088

Table IIIb: parallel double inverted pendulum

RMSE for the estimation performed by the H-infinity KF$\times 10^{-6}$

	$RMSE_{x_1}$	$RMSE_{x_2}$	$RMSE_{x_3}$	$RMSE_{x_4}$
test_1	0.6731	0.0340	0.7262	0.0519
test_2	0.5715	0.0340	0.7832	0.0519
test_3	0.7891	0.0341	0.8096	0.0519
test_4	0.7732	0.0340	0.4383	0.0519
test_5	0.6005	0.0341	0.7095	0.0519
test_6	0.7819	0.0340	0.7099	0.0519
test_7	0.9036	0.0340	0.5537	0.0519
test_8	0.9088	0.0341	0.7757	0.0519

Table IVb: parallel double inverted pendulum

Convergence time (sec) for state variables x_1 to x_4

	T_s x_1	T_s x_2	T_s x_3	T_s x_4
test_1	10.0	4.0	10.0	4.0
test_2	9.0	3.5	9.0	3.5
test_3	12.0	4.0	12.0	4.0
test_4	10.0	3.5	10.0	3.5
test_5	12.0	3.5	12.0	3.5
test_6	11.0	3.5	11.0	3.5
test_7	10.0	3.5	10.0	3.5
test_8	7.5	4.0	7.5	4.0

Comparing to past approaches for treating the nonlinear optimal (H-infinity) control problem, the article's approach is applicable also to dynamical systems which have a non-constant control inputs gain matrix. Furthermore, it uses a new Riccati equation to compute the controller's gains and follows a novel Lyapunov analysis to prove global stability for the control loop. It is also noteworthy that the nonlinear optimal control method is applicable to a wider class of dynamical systems than approaches based on the solution of State Dependent Riccati Equations (SDRE). The SDRE approaches can be applied only to dynamical systems which can be transformed to the Linear Parameter Varying (LPV) form. Besides, the nonlinear optimal control method performs better than nonlinear optimal control schemes which use approximation of the solution of the Hamilton-Jacobi-Bellman equation by Galerkin series expansions. The stability properties of the Galerkin series expansion -based optimal control approaches are still unproven.

Moreover, to provide a comparison between the article's nonlinear optimal control method and NMPC it can be noted that the computational burden of NMPC comes from a sequential optimization procedure which mostly relies on gradient-based algorithms. Therefore, the complexity for computing the control inputs at each sampling instance may come from calculating the elements of Jacobian matrices and the associated gradient functions. However, the main flaw of NMPC is the lack of global stability proof. It is not always ensured that NMPC's iterative search for the optimum will be convergent. Often the performance of this optimization procedure is based on initial conditions (multiple shooting methods) and on empirical selection of coefficients for the cost function and the control inputs.

The article's nonlinear optimal (H-infinity) control method is of proven global stability and its convergence to the optimum is little dependent on parameter values selection. There are three parameters in the method's algebraic Riccati equation, namely gains r, ρ and Q which affect the accuracy of setpoints tracking and transient performance, with variation ranges that can be selected on the basis of offline simulation experiments. The proposed nonlinear optimal control method is of global (and not local) stability properties. This is explicitly proven through Lyapunov stability analysis. The article's Lyapunov stability proof makes use of the tracking error dynamics of the initial nonlinear system. The computed control inputs are applied to the initial nonlinear model of the rotary double inverted pendulum and not to its linear approximation. It is ensured that the linearization error due to truncation of higher-order terms in the Taylor-series expansion remains small because the linearization process is performed at each sampling period around the present value of the rotary double inverted pendulum's state vector and not at a point on the desirable trajectory. By taking the span between the linearization point and the system's state vector at each sampling period to be small one concludes that the model which is obtained from linearization describes with precision the initial nonlinear dynamics of the pendulum. This is also proven in detail through Eq. (25) to Eq. (27) which appear in subsection 3.1 of the article.

Finally, about the real-time implementation of the nonlinear optimal (H-infinity) control scheme this is absolutely feasible because the solution of the method's algebraic Riccati equation and the associated computation of the optimal control inputs (with Matlab's aresolv() function or with equivalent Riccati equation solvers) is performed in a very small time-interval which is significantly smaller than the sampling period. Shortening further the computation time of the nonlinear optimal control method during each time-step of the control algorithm is dependent on more efficient Riccati equations solvers and this is even nowadays an open research topic. Finally, about the performance of the H-infinity Kalman it can be noted that this estimator performs better than the Extended Kalman Filter in terms of robustness and accuracy of the provided state estimates under raised levels of measurement noise.

8 Conclusions

The rotary double inverted pendulum (double Furuta's pendulum) is a benchmark nonlinear dynamical system and the solution of the associated control problem provides significant insight towards treating also

the nonlinear control problem in several underactuated robotic systems. The article has proposed a new nonlinear optimal control method for the dynamic model of the double rotary pendulum. This control problem exhibits high difficulty because of its highly nonlinear dynamic model, as well as because of underactuation. First, the dynamic model of the rotary double inverted pendulum has undergone linearization with the use of first-order Taylor series expansion and through the computation of the associated Jacobian matrices. The linearization process was taking place at each sampling instance, around a temporary operating point which was defined by the present value of the pendulum's state vector and by the last sample value of the control inputs vector. For the approximately linearized model of the system an H-infinity feedback controller was designed.

This H-infinity controller offers a solution of the optimal control problem for the dynamic model of the rotary double inverted pendulum under model uncertainty and external perturbations. Actually, it represents a min-max differential game taking place between the (i) the controller which tries to minimize a cost function that contains a quadratic term of the state vector's tracking error (ii) the model uncertainty and exogenous perturbation terms which try to maximize this cost function. To select the feedback gains of the H-infinity controller an algebraic Riccati equation had to be solved repetitively at each time-step of the control algorithm. The global stability properties of the control scheme have been proven through Lyapunov analysis. First, the H-infinity properties of the control have been proven which have demonstrated the method's robustness against model imprecision and disturbances. At a second stage global asymptotic conditions for the control loop have been reached. To implement state estimation-based control without the need to measure the entire state vector of the rotary double inverted pendulum, the H-infinity Kalman Filter has been used as a robust state estimator. The nonlinear optimal control method retains the advantages of linear optimal control, that is fast and accurate tracking of reference setpoints under moderate variations of the control inputs. The efficiency of the nonlinear optimal control method for a wide class of underactuated nonlinear optimal control method has been also confirmed, with the parallel double inverted pendulum to be another case study.

Declarations: The authors of this article confirm that (i) to their knowledge no conflict of interest exists with third parties about the content of the present manuscript (ii) The contribution of the authors to this research work is designated by their order of appearance in the article's list of authors (iii) Computation data for this manuscript are available by the corresponding author upon reasonable request.

References

[1] G. Rigatos, Nonlinear control and filtering using differential flatnesss theory approaches: Applications to electromechanical systems, Springer, 2016

[2] G. Rigatos and K. Busawon, Robotic manipulators and vehicles: Control, estimation and filtering, Springer, 2018

[3] G. Rigatos and E. Karapanou, Advances in applied nonlinear optimal control, Cambridge Scholar Publishing, 2020

[4] G. Rigatos, M. Abbaszadeh, P. Siano, Control and estimation of dynamical nonlinear and partial differential equation systems: Theory and Applications, IET Publications, 2022

[5] T. Kobayashi, M. Iwase, S. Suzuki and K. Furuta, Swinging-up and balancing control of double Furuta pendulum by using State Dependent Riccati Equation, IFAC 2004 Conference on Mechatronic Systems, Sydney, Australia, 2004

[6] K. Nagachi, M. Izatsu, N. Kamamichi. T. Shiotsuki, J. Ishikawa and K Furuta, Swinging-up and balancing control of double Furuta pendulum by using State Dependant Riccati Equation, IEEE/RSJ 2009 Intl. Conf. on Intelligent Robots and Systems, St. Louis, USA, Oct. 2009

[7] M. Matsuda, M. Izursu and K. Furuta, Simultaneous swinging-up and stabilization of double Furuta pendulum, IEEE SICE 2007, Kagawa University, Japan, Sep. 2007.

[8] Z. Wang, L.B/ Freidovich and M. Zhang, Periodic motion planning and control for double rotary perndulum via virtual balancing constrains, IEEE/CAA Journal of Automatica Sinica, vol. 6, no. 1, pp. 291-298, 2019.

[9] N. Matsuda, M. Izutsu and K. Furuta, Simultaneous swinging-up and stabilization of double Furuta pendulums. IEEE SICE 2007 Conference, Kagawa, Japan, Sep. 2007

[10] T. Henmi, M. Deng and A. Inoue, Unified method for swing-up control of double inverted pendulum systems, IEEE AIMS 2014, IEEE 2014 Conference on Advanced Mechatronic Systems, Kumamoto, Japan, Aug. 2014

[11] J. Ismail and S. Liu, Efficient planning of optimal trajectory for a Furuta double pendulum using discrete mechanics and optimal control, 20th IFAC World Conference, Toulouse, France, July 2017.

[12] R.W. Brockett and M. Li, A light weight rotary double pendulum: maximizing the domain of attraction, IEEE CDC 2007, IEEE 42nd Conference on Decision and Control, Maui, Hawai, USA, Dec. 2003

[13] T. Komine, M. Iwase, S. Suzuki and K. Furuta, Rotational control of double pendulum, IFAC 2004 on Mechatronic Systems, Sydney, Australia, 2004

[14] J. Yu and X. Zhang, The global control of first-order rotary parallel double inverted pendulum system, IEEE CCC 2021, IEEE 40th Chinese Control Conference, Shanghai, China, July 2021.

[15] T.S. Amer, M.A. Bek, M.S. Nael, M.A. Sirwah and A. Arab, Stability of the dynamical motion of a damped 3-DOF autoparametric pendulum system, Journal of Vibration Engineering & Technologies, Springer 1-21, 2022

[16] S.D.A Sunjeewa and M. Parnichkun, Control of rotary double inverted pendulum system using LQR sliding surface based sliding-mode controller, Journal of Control and Decision, Taylor and Francis, vol. 9, no. 1, pp. 89-101, 2022

[17] H. Hoang and M. Wengsaisuwan, Robust controller design for a rotary double inverted pendulum using Linear Matrix Inequalities, IEEE SICE 2007 Conferences, Kagawa University, Japan, Sep. 2007

[18] S.S. Sanjeewa and M. Parnichkun, Control of rotary double inverted pendulum system using mixed sensitivity H_∞ control, Intl. Journal of Advanced Robotic Systems, Sage Publications, March-April 2019. pp. 1-17

[19] N. Dakovic and M. Radulovich, Flatness and LQR control of Furuta pendulum, ETF Journal of Electical Engineering, vol. 21, no. 1, pp.. 138-146, 2015

[20] Z.B. Hazem, M.J. Fotuhi and Z. Bingul, A study of anti-swing fuzzy LQR control for a double serial link rotary pendulum, IETE Journal of Research, Taylor and Francis, pp. 1-13, 2021

[21] M. Patil and S. Kurode, Stabilization of rotary double inverted pendulum using high-order sliding-modes, IEEE ASCC 2017. IEEE 2017 11th Asian Control Conference, Gold Coast Convention Center, Australia, Dec. 2017.

[22] H. Patil and S. Kurode, Stabilization of RDIP using sliding modes, IEEE ICC 2018, IEEE 2018 Indian Control Conference, Jan. 2018. Kanpur, India

[23] A. Jabbari, F.M. Malik and S.A. Sheikh, Nonlinear stabilizing control of a rotary double inverted pendulum: a modified backstepping approach, Transactions of the Institute of Measurement and Control, Sage Publications, vol. 38, no. 11, pp. 1721-1734, 2017.

[24] I.M. Mehedi, U.M. Al-Saggaf, R. Mansouri and M. Bettayeb, Stabilization of a double inverted rotary pendulum through fractional-order integral control scheme, International Journal of Advanced Robotic Systems, Sage Publications, pp. 1-9, July-Aug. 2019.

[25] J. Yu and X. Zhang, The global control of first-order rotary parallel double inverted pendulum system, IEEE CCC 2021, IEEE 40th Chinese Control Conference, Shanghai, China, July 2021.

[26] A. Fradkov, B. Andrievsky and K. Boyko, Control of the coupled double pendulum systems, Mechatronics, Elsevier, vol. 15, pp. 1289-1303, 2005.

[27] M. Alamir and A. Murilo, Swing-up and stabilization of a twin pendulum under state and control constraints by a fast MPC scheme, Automatica, Elsevier, vol. 44, pp. 1319-1324, 2008

[28] E. Arondo-Escolastico, M. Guinaldo, M. Santos and S. Dormido, Control of a chain pendulum: A fuzzy logic approach, Inlt. Journal of Computational Intelligence Systems, Taylor and Francis, vol. 9, no. 2, pp. 281-295, 2016

[29] L. Fan, A. Zhang, G. Pan, Y. Du and J. Qiu, Swing-up and fixed-time stabilization control of underactuated cart-double pendulum system, IET Control Theory and Applications, pp. 1–10, 2022.

[30] M.F. Hamza, H.J. Yap, I.A. Choudhury, A.I. Isa, A.Y. Zimit and T. Kumbasar, Current development on using Rotary Inverted Pendulum as a benchmark for testing linear and nonlinear control algorithms, Mechanical Systems and Signal Processing, Elsevier, vol. 116, pp. 347–369, 2019

[31] N.P. Nguyen, H. Oh, Y. Kim, J. Moon, J. Yang and W.H. Chen, Fuzzy-Based Super-Twisting Sliding Mode Stabilization Control for Under-Actuated Rotary Inverted Pendulum Systems, IEEE Access, vol. 8, pp. 185079-185093, 2020.

[32] I. Mehedi1, U, Ansari, A. Bajodah, U.M. AL-Saggaf, B. Kada and M.J. Rawa, Underactuated rotary inverted pendulum control using robust generalized dynamic inversion, Journal of Vibration and Control, Sage Publications, vol. 26(23–24) 2210–2220, 2020.

[33] D. Cruz-Ortiz, M. Ballesteros, A. Polyakov, D. Efimov, I. Chairez and A. Poznyak, Practical Realization of Implicit Homogeneous Controllers for Linearized Systems, IEEE Transactions on Industrial Electronics, vol 69, no. 5, pp. 5142-5151, 2021,

[34] Y. Fujita, M. Izutsu and S. Hatakeyama, Swing-Up and Stabilization Control of Twin Furuta Pendulums by Energy Control, IEEE IECON, 2014, IEEE 40th Annual Conference of the IEEE Industrial Electronics Society, Dallas, Texas, Oct. 2014

[35] A. Ibeas; A. Esmaeili, J. Herrera and F. Zouari, Discrete-time observer-based state feedback control of heart rate during treadmill exercise, IEEE ICSTCC 2016, IEEE 20th International Conference on System Theory, Control and Computing, Sinaia, Romania, Oct. 2016

[36] L. Merazka, F. Zouari and A. Boulkroune, Fuzzy state-feedback control of uncertain nonlinear MIMO systems, IEEE ICSC 2017, IEEE 2017 6th International Conference on Systems and Control, Batna, Algeria, May 2017

[37] L. Merazka; F. Zouari; A. Boulkroune, High-gain observer-based adaptive fuzzy control for a class of multivariable nonlinear systems, IEEE ICSC 2017, IEEE 2017 6th International Conference on Systems and Control, Batna, Algeria, May 2017

[38] G. Rigatos, A differential flatness theory approach to observer-based adaptive fuzzy control of MIMO nonlinear dynamical systems, Nonlinear Dynamics, Springer, vol. 76, no. 2, pp. 1335-1354, 2014.

[39] F. Zouari, K, Ben-Saad and M. Benrejeb, Adaptive backstepping control for a single-link flexible robot manipulator driven DC motor, IEEE CoDIT 2013, IEEE 2013 International Conference on Control, Decision and Information Technologies, Hammamet, Tunisia, May 2013

[40] G. Rigatos, P. Siano and M. Abbaszadeh, Nonlinear H-infinity control for 4-DOF underactuated overhead cranes, Transactions of the Institute of Measurement and Control, Sage Publications, 2017.

[41] G.G. Rigatos and S.G. Tzafestas, Extended Kalman Filtering for Fuzzy Modelling and Multi-Sensor Fusion, Mathematical and Computer Modelling of Dynamical Systems, Taylor & Francis (2007), 13, pp. 251-266.

[42] M. Basseville and I. Nikiforov, Detection of abrupt changes: Theory and Applications, *Prentice-Hall*, 1993.

[43] G. Rigatos and Q. Zhang, Fuzzy model validation using the local statistical approach, Fuzzy Sets and Systems, Elsevier, vol. 60, no. 7, pp. 882-904,2009.

[44] G.J. Toussaint, T. Basar and F. Bullo, H_∞ optimal tracking control techniques for nonlinear underactuated systems, in Proc. IEEE CDC 2000, 39th IEEE Conference on Decision and Control, Sydney Australia, 2000.

[45] M. Deng, A. Inoue, T. Henmi and N. Ueki Analysis and experiment on simultaneous swing-up of a parallel cart-type double inverted pendulum, Asian Journal of Control, J. Wiley, vol. 10, no. 1, pp. 121-128, 2008

[46] T. Henmi, m. Deng and A. Inoue, Unified method for Swing-up Control of Double Inverted Pendulum Systems, IEEE AMS 2014, Proc. of the 2014 International Conference on Advanced Mechatronic Systems, Kumamoto, Japan, Aug. 2014.

[47] M. Deng, A. Inoue, S. Nakagawa, T. Henmi, N. Ueki, and Y. Hirashima, Experimaental study on simultaneous swing-up of parallel double inverted pendulum, Proc. of the 23rd Chinese Control Conference, pp.1627-1631, 2004.